The International Journal of Advanced Manufacturing Technology
https://doi.org/10.1007/s00170-024-13071-3

CRITICAL REVIEW

Residual stress measurement in engine block—an overview

Houman Alipooramirabad[1,2] · Sina Kianfar[2] · Anna Paradowska[3,4] · Reza Ghomashchi[5]

Received: 28 July 2023 / Accepted: 18 January 2024

Abstract
Significant residual stresses are often generated during the manufacturing of cast Al-Si alloy engine blocks due to differential cooling rates, the mismatch in the thermo-physical properties of adjacent materials in direct contact and volumetric changes caused by solid-state phase transformations during cooling. These may be modified during heat treatment and operation. These residual stresses may lead to distortion (affecting performance and economy) or premature failure of the engine block. For this reason, it is of fundamental importance to have reliable numerical and experimental methods for characterizing the residual stresses in the engine blocks at several steps during the manufacturing process. Sectioning and neutron diffraction techniques have been widely used to determine the residual stresses in the engine blocks. Numerical techniques have been developed to predict these residual stress but require experimental validation. The authors reviewed several numerical and experimental studies of residual stress evolution in engine blocks and showed how the residual stresses, microstructures, and mechanical properties are correlated.

Keywords Residual stress · Engine block · Neutron diffraction · Aluminum casting,· Finite element Modelling · Heat treatment · Sectioning technique

1 Introduction

Residual stresses, by definition, are "self-balancing" and "locked-in" stresses that remain in the material and structures after processing or manufacture in the absence of external forces. Residual stresses are often generated during manufacturing (particularly casting, welding, and forming) and can also occur during service. Residual stresses can significantly affect the dimensional stability, material strength, and fatigue life of major structural components such as airplanes, bridges, and ships [1–3]. Despite their fundamental importance, residual stresses are often underestimated or overlooked in the engineering components as they occur in the absence of any external loads. Mechanisms for generating residual stresses include non-uniform plastic deformation, which occurs in forming processes (such as forging and rolling), surface modification (i.e., grinding or shot peening), from thermal stresses from large thermal gradients (e.g., welding, casting) [4–7], or from thermal expansion mismatch between materials (such as gray cast iron cylinder liner with flake graphite cast into an Al-Si engine block).

For cast components, in general, residual stresses can be generated during the solidification of molten alloy and subsequent cooling process mainly due to the temperature gradients between different parts of casting, the different thermal expansion of adjacent components, or a restrained mold or liner imposing mechanical loads during the shrinkage of the cast material [8–10]. For the engine blocks, which are the focus of this paper, the development of residual stress is mainly due to thermal gradients caused by differences in cooling rates that occur during the casting operation and a mismatch in the coefficient of thermal expansion (CTE) in multi-material engine blocks produced with Al-Si alloys and gray cast-iron liners [11, 12]. The difference in cooling rate can occur due to several factors, including complex casting

✉ Houman Alipooramirabad
houman.amirabad@gmail.com

1 Collegue of Engineering, Birmengham City University, 15 Bartholomew Row, Birmingham B5 5JU, UK

2 School of Engineering, University of British Columbia, Okanagan, BC V1V 1V7, Canada

3 Australian Nuclear Science and Technology Organisation (ANSTO), Lucas Heights, Sydney, NSW 2234, Australia

4 School of Civil Engineering, the University of Sydney, Sydney 2006, Australia

5 School of Mechanical Engineering, the University of Adelaide, Adelaide, SA 5005, Australia

Published online: 31 January 2024

geometry, thickness variation, and localized placement of chills in the casting setup [13, 14]. The magnitude of tensile residual stress may surpass the yield strength of the material and lead to distortion, particularly in cylinder bores, and increase the susceptibility of cracking during operation, where it is exposed to fatigue and elevated temperature. Therefore, residual stress measurement in the engine blocks, which operate under high applied thermo-mechanical loading, is of fundamental importance.

During casting, heat flow from thicker sections is slower and may lead to thermal mismatch stresses, void formation in the thickest sections, and possibly segregation of the alloy composition. Cast-in iron liners (typically of gray cast iron with flake graphite) lead to significant stresses as the coefficient of thermal expansion of the Al is ~ twice that of Fe. The stresses develop when cooling from the temperature where the yield strength of Al exceeds the thermal mismatch stress down to room temp. Generally, there is a thicker section of Al than of the Fe, so there will be high compressive stresses in the gray cast iron liner and lower tensile stresses in the Al-Si alloy in the cylinder bridge.

The thickest sections in the Al-Si alloy have two problems. Tri-axial tensile stresses can be high without yielding (they can go above yield), which can lead to fracture. Also, thicker sections are the last to freeze during casting, and most casting defects will occur here. The only saving grace is that, due to the thicker section, the imposed stresses tend to be lower.

There are several experimental and numerical methods for evaluating residual stress in cast components, particularly engine blocks. The numerical techniques all require extensive material testing across a range of temperatures, extensive modelling, and measurement to find the correct temperature history across the model, and these residual stress predictions then require validation from experimental measurements.

Experimental measurement techniques are broadly categorized into destructive (i.e., hole drilling, indentation, and sectioning techniques) and non-destructive methods (e.g., and neutron or X-ray diffraction) [15]

In destructive methods, the specimen is drilled or cut mechanically to measure the strain due to the stress-relaxation generated in the component upon the material removal [16]. In contrast, non-destructive methods (diffraction techniques) are based on the Bragg's law to measure residual stresses from the changes in the interplanar spacing of the restrained (stressed) and non-restrained (stress-free) samples. The processing and chemical composition of the stress-free sample must be identical to those of the stressed one [17–19] but is cut from an identical component, where the cutting removes the restraint and thus removes the residual stress. In this case, the lattice plane acts as a built-in strain gauge inside materials, by comparing the stressed and stress-free samples. These non-destructive methods are ideal candidates for the residual stress measurements as they are able to measure the stress state of the material at a number of internal positions in contrast to destructive, cutting/sectioning techniques which are typically limited in where the stress is assessed.

It is important to highlight that long-range macroscopic stresses (referred to as type I stresses) are measured in the engine block by these measurement techniques (types II and III are stresses which arise from grain-to-grain anisotropy or sub-grain-scale stresses arising from defects, precipitates, and dislocations [20]). The sampling gauge volume is considerably larger than the grain size, typically covering thousands of individual grains, so only type I macro stress is measured.

In addition to experimental techniques, numerical modelling employing finite element methods (FEM) are viable tools for predicting and analyzing residual stress generation during the manufacturing process of cast powertrain components like engine blocks and cylinder heads [11, 21]. Early assessment of the residual stresses at the design stage (prior to mass production) enables engine developers and manufacturers to determine resistance to deformation or cracking after considering the combined effects of both residual stress and in-service operating stress. The design and/or manufacturing of engine block can be optimized accordingly in cases where high residual stress exists [22, 23]. Therefore, the detrimental effects of residual stresses in internal combustion engines (ICEs) will be alleviated, resulting in more efficient and environmentally friendly vehicles.

This report focuses on the experimental and numerical residual stress measurements in engine blocks. In this paper, the authors summarize:

(i) The theoretical basis of destructive measurements (i.e., cutting or slitting) to measure residual stresses in the engine block with the focus on macroscopic or type I residual stress
(ii) The theoretical basis of neutron diffraction measurements to measure residual stresses in the engine block with the focus on macroscopic or type I residual stress
(iii) A survey of experimental methods (neutron diffraction and sectioning technique) on residual stress measurements in engine blocks
(iv) The theoretical basis of numerical modelling with conducted research on the prediction of residual stresses in casting (benchmark studies) and engine blocks

2 Experimental measurement techniques

2.1 Destructive technique

The destructive techniques are called stress-relaxing methods, which measure the micro distortion due to the release of

the residual stress generated in the material upon its removal [1]. Measuring the macroscopic strains by removal of the material (e.g., cut, drilled, or bored) from a specimen with residual stresses is the basis of any destructive technique used to measure the residual stress. There are several well-established destructive methods to measure the residual stresses, including sectioning [24], the contour method [25], curvature measurements [26], hole drilling [27], crack compliance [28], and ring core methods [29]. Only the sectioning technique will be discussed in this paper as there are limitations with other destructive techniques to quantify residual stresses in engine blocks with complex geometries.

2.1.1 Sectioning technique

The sectioning method is a fully destructive test that involves cutting a component with strain gauges attached to quantify the residual stresses. The sectioning technique is simple and cost-efficient and can be applied to most alloys and metals. In this method, strain gauges are attached to the surface of the component which detect the displacement that results from stresses released during cutting. The cutting can be done by milling [30], wire cutting [31], or band sawing [32] to ensure that the residual stresses in the specimen relax completely [6]. The cutting process should be done without introducing any heat or plastic deformation, so that an accurate measurement of residual stress/strain can be made without any plasticity effects [10]. Unlike neutron diffraction, this technique can only show local stresses in the direction of the strain gauge.

Mechanical characterization of residual stresses in the sectioning technique is dependent on the strain gauges used for measuring the deformation caused by the relaxation of residual stresses. Depending on the application, different types of strain gauges can be used (i.e., uniaxial, bi-axial, or tri-axial strain gauges), enabling strain measurements in different directions. Strain gauges measure the deformation of the material through the changes encountered in their electrical resistance. The strain measurements can be done in the microstrain scales, which induce tiny changes in the strain gauge resistance. Therefore, an accurate determination of electrical resistance is required for the precise strain measurements. For that purpose, a Wheatstone bridge is utilized to magnify the strain gauge electrical resistance. The Wheatstone bridge is an electrical circuit containing a voltage excitation (V_{ex}) and four resistances, as shown in Figure 1 [33]. When all resistances are equal, the voltage output (V_o) will be zero, and the bridge is said to be balanced. Any changes in resistance in any arm of the bridge will result in a non-zero output voltage, according to Eq. (1):

$$Vo = V_{ex}(R_1R_3 - R_2R_4)/(R_2 + R_1)(R_3 + R_4) \quad (1)$$

The output voltage (V_o) is characteristic of the deformation. Each strain gauge needs to be included in a Wheatstone bridge. As mentioned before, the strains expected from sectioning are very small and cannot be measured with sufficient accuracy using conventional industrial equipment. A specialized data acquisition system is, therefore, required where each strain gauge is connected to a Wheatstone bridge circuit with three control gauges.

The strain gauges need to be applied carefully on cleaned metal, as described in [22].

2.1.2 Applications of sectioning technique to measure residual strains/stresses in engine block

Kianfar et al. [32] utilized the sectioning method to investigate the effects of the high-pressure die casting (HPDC) process on the residual stress evolution of an inline-4 (I4) Al-Si alloy engine block with cast-in gray cast iron liners with flake graphite in conjunction with microstructural and mechanical properties studies. Figure 2 shows the strain gauges mounted at different locations of the engine block in the hoop and axial directions with the summary of measured residual strains (με) for each location of interest in the Al

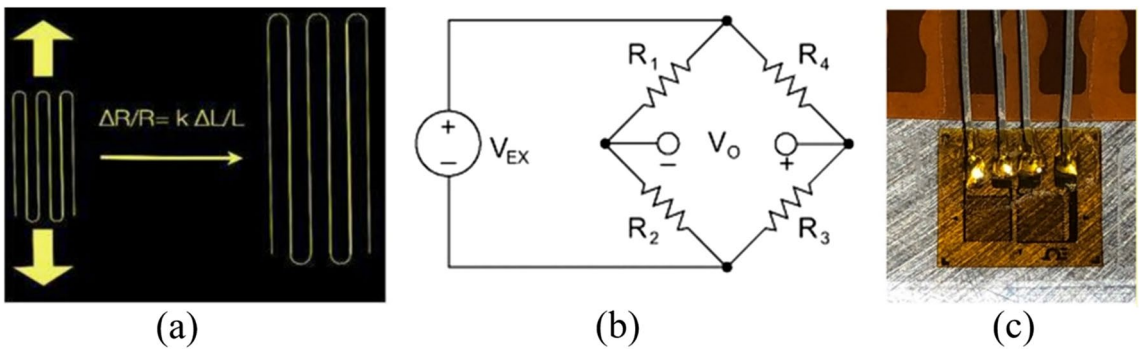

Fig. 1 Operating principle of strain gauges, **a** change in length changes the resistance, **b** Quarter Wheatstone bridge [84], **c** an applied strain gauge for the sectioning method [33]

cylinder bridge (CB) and gray cast iron liner. Compressive residual stress of 450 MPa was measured in the axial direction of the gray cast iron liner, balanced by lower tensile residual stresses in the Al CB, which was equivalent to about 70% of the alloy's yield strength (the yield strength of the Al-Si alloy at the top of the CB was 212 MPa). There were variations in the engine block's mechanical properties along the CB, with the higher yield and tensile strength at the top of the cylinder compared to the base. The yield and tensile strength at the top of the cylinder were 15% and 8% greater than at the base, respectively. Such changes were associated with the higher cooling rate experienced at the top of the cylinder confirmed by the metallographic analysis (the degree of microstructural refinement was found to be higher at the top as compared to the bottom).

Mohammed et al. [34] utilized the sectioning technique to measure the evolution of residual strain and stress in I4 sand-cast Al-Si (319, Al–Si–Cu alloy) engine blocks subjected to different heat treatment conditions. The heat treatments were initiated with solution heat treatment followed by quenching in a different media (warm and cold-water quenching) and sub-zero cooling to −30 °C. The engine block was then aged applying T6 and T7 aging treatments. Residual stress measurements were conducted in different heat treatment phases, as shown in Figure 3.

The cutting sequence as well as the experimental setup for the residual stress measurements is represented in Figure 4.

A substantial reduction in the magnitude of tensile residual stresses was observed after solution heat treatment, quenching, and sub-zero treatment (i.e., from 105 MPa in the

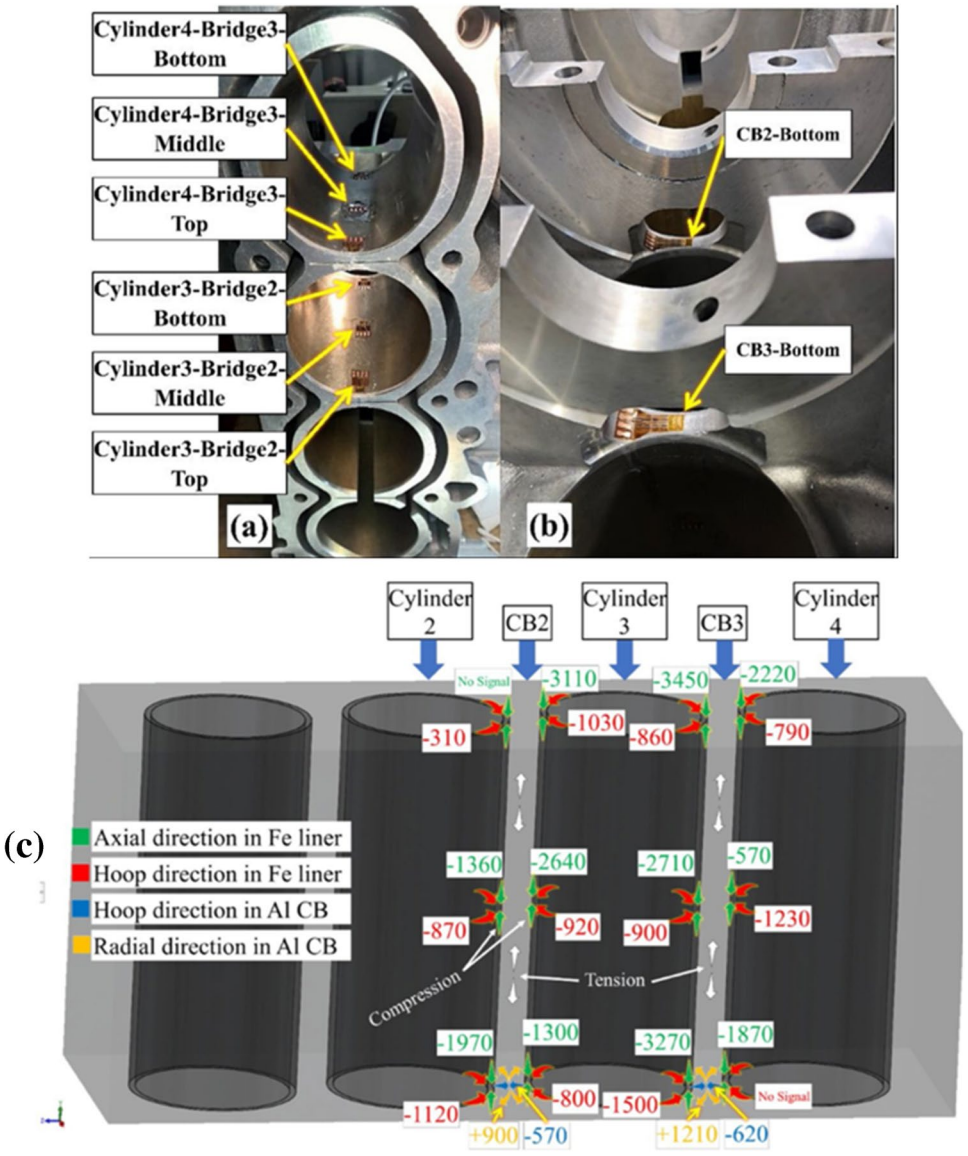

Fig. 2 The strain gauge locations in **a** the gray cast iron liners with flake graphite, **b** the bottom of the bridges, and **c** a summary of measured strain (με) for the locations of interest in the cylinder bridge of Al-Si alloy part and gray cast iron liner [32]

as-cast state to 52 Mpa after the cryogenic treatment). Also, further stress relief was observed after cyclic freezing, while freezing time had no significant effect on stress relief. The freezing condition effects with different quenching rates are shown in Figure 5.

Similar to previous observations [35–38], the aging temperature was found to be a controlling parameter in residual stress relaxation (T7 aging treatment at 250 °C mitigates the residual stresses substantially compared to T6 aging at a temperature of 170 °C with no significant stress relieving effects). This could be attributed to the precipitate coarsening and coherency loss but is likely to be dislocation creep at higher temperatures [34].

Carrera et al. [12] measured the residual stresses in sand-cast engine blocks using the sectioning method with mounted strain gauges. Tensile residual stresses (~150 Mpa) were found in the cylinder bridge of the Al-Si alloy engine block with gray cast iron liners (cast-in), while the engine blocks without liners exhibited compressive stresses of 20 Mpa in the CB. It was observed that the residual stresses were affected by the engine block dimensions and, particularly, the cylinder bridge thickness, where residual stresses decrease as the thickness increases. Higher residual stresses were found in the V8 engine blocks compared with the I4 blocks with similar wall thickness. These observations correlate well with the numerical results of Su et al. [11], who utilized strain gauges to measure the residual stresses and validate the FEM results. It was found that the cylinder bridge is the most critical location in an Al-Si alloy engine block containing a gray cast iron liner with respect to the residual stress magnitude [12]. This is mainly because the contraction/expansion of the Al material in the cylinder bridge area is restricted by two adjacent liners, increasing residual stress [11, 12].

Aguilar-Navarro et al. [22] utilized both sectioning and indentation techniques with a strain gauge to measure residual stresses along the bridge in a V8 engine block. In the indentation technique, a pair of indentation marks was made by a gauge punch in the study section which is followed by a cutting process, as shown in Figure 6. The strain can then be calculated through the difference between indentation distance before and after stress relief by the cutting process. A comparative analysis was conducted between the two methods; the difference between the methods was 3.9%, which indicates the effectiveness of the indentation technique for residual stress measurements in complex areas (residual stresses of 69.94 MPa and 67.21 MPa were found by the strain gauge and indentation techniques respectively).

The sectioning method has proven to be accurate and economical specifically for the relatively small wall thickness

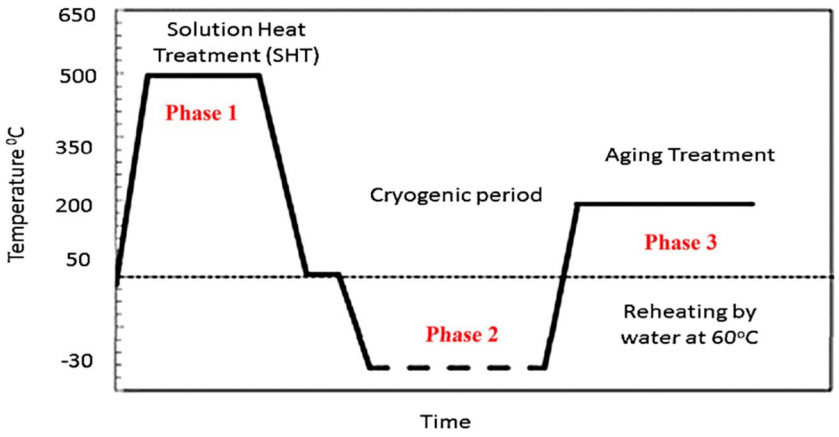

Fig. 3 Different steps involved with the heat treatment with their corresponding residual stress measurements [34]

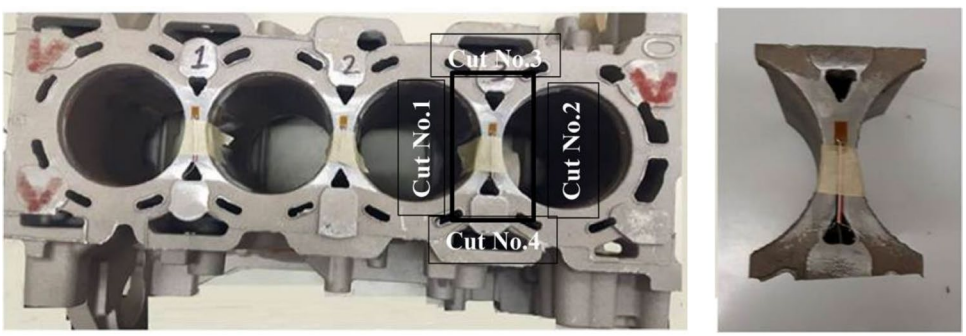

Fig. 4 The experimental set up and cutting sequence **a** before sectioning and **b** after sectioning for strain measurement using the sectioning technique [34]

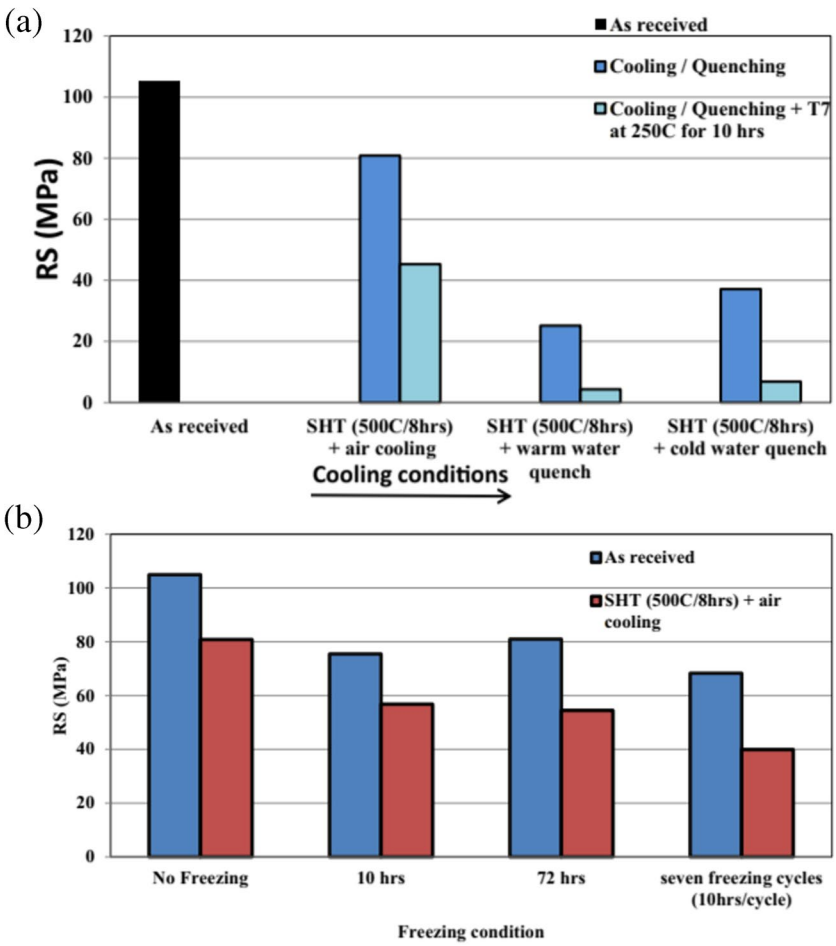

Fig. 5 Residual stress development with **a** different quenching rates and **b** freezing condition effects in I-4 engine block [34]

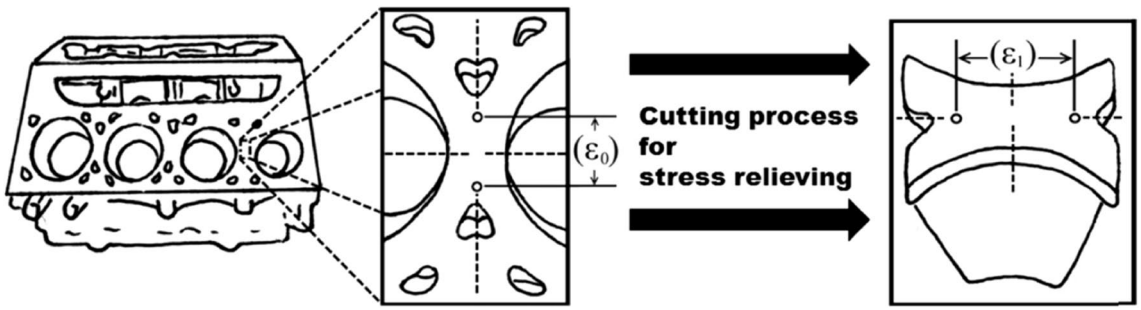

Fig. 6 Schematic diagram of indentation marks before (ε_o) and after (ε_1) stress relieving by the cutting process [22]

structures (i.e., the Al-Si alloy part of CB or the gray cast iron liner) if proper care is taken for specimen preparation and measurement procedure [16, 39, 40].

The destructive techniques which involved slitting gave residual stress measurements in limited locations only, unlike neutron diffraction. The technique was able to measure stresses in different materials (Al-Si alloy and gray cast iron liner) which is not possible with neutron diffraction without changing the wavelength/energy of the incoming neutron beam. The slitting technique is also a useful confirmation of more detailed neutron techniques and of numerical techniques.

2.2 Non-destructive residual stress measurements (neutron diffraction techniques)

2.2.1 Background and theoretical basis

Neutron diffraction (ND) is a non-destructive technique for measuring residual stresses in many situations, including

engineering components with $\pm 50 \times 10^{-6}$ accuracy in strain with > 0.1 mm spatial resolution [19, 41–44]. ND utilizes neutrons generated by fission or spallation processes at nuclear research facilities. The neutrons in both cases need to be moderated (using heavy water) and bring their energy levels to the thermal range; this allows the combination of wavelength (which is equivalent to the neutron's energy) and the inter-planar spacing of the metal to define a scattering angle which is convenient for experimental use in steady-state research reactors where nuclear fission produces continuous neutron beams, as shown in Figure 7a; the neutron beam needs to be of a single wavelength (or energy) which is achieved by the placing a single crystal monochromator in the beam path to only diffract neutrons of a specified wavelength. The neutron beam with the specific wavelength (monochromated beam) is then defined to project in a specific direction by slits and a collimator. The beam from the collimator is then used as the incident beam in the ND experiment.

An alternative method of producing neutrons is spallation which is based on nuclear reactions that occur when high-energy subatomic particles (for example, protons or neutrons) interact with an atomic nucleus. Short pulses of neutrons are then produced by periodic bombardment of an atomic nucleus by high energy particles, the neutrons have a spread of wavelengths that arrive at the sample over a short period of time, as can be seen in Figure 7b–d [18, 45–47]. The neutron energy and therefore wavelength can be determined on detection from the traveling distance and the time-of-flight (TOF). TOF measurements are, therefore, energy-dispersive, with the entire diffraction pattern recorded at any particular scattering angle. Utilizing a pulsed beam source with the simultaneous observation of multiple peaks also enables studying the texture, phase change, and in situ deformation behavior in many polycrystalline materials [45] as well as allowing stress measurements in two directions simultaneously. None of the papers in this review used a spallation source, but this technique is regularly used for residual stress measurement of engineering components and is suitable for use on engine blocks.

2.2.2 Theoretical background

The principle of ND for the residual strains/stresses measurement is based on Bragg's law:

$$n\lambda = 2d \sin \theta \tag{2}$$

where n is the diffraction order, λ is the wavelength of the incident neutron beam, d is the spacing between two adjacent atomic planes within the crystal structure of the material, and the scattering angle, 2θ, is the diffraction angle

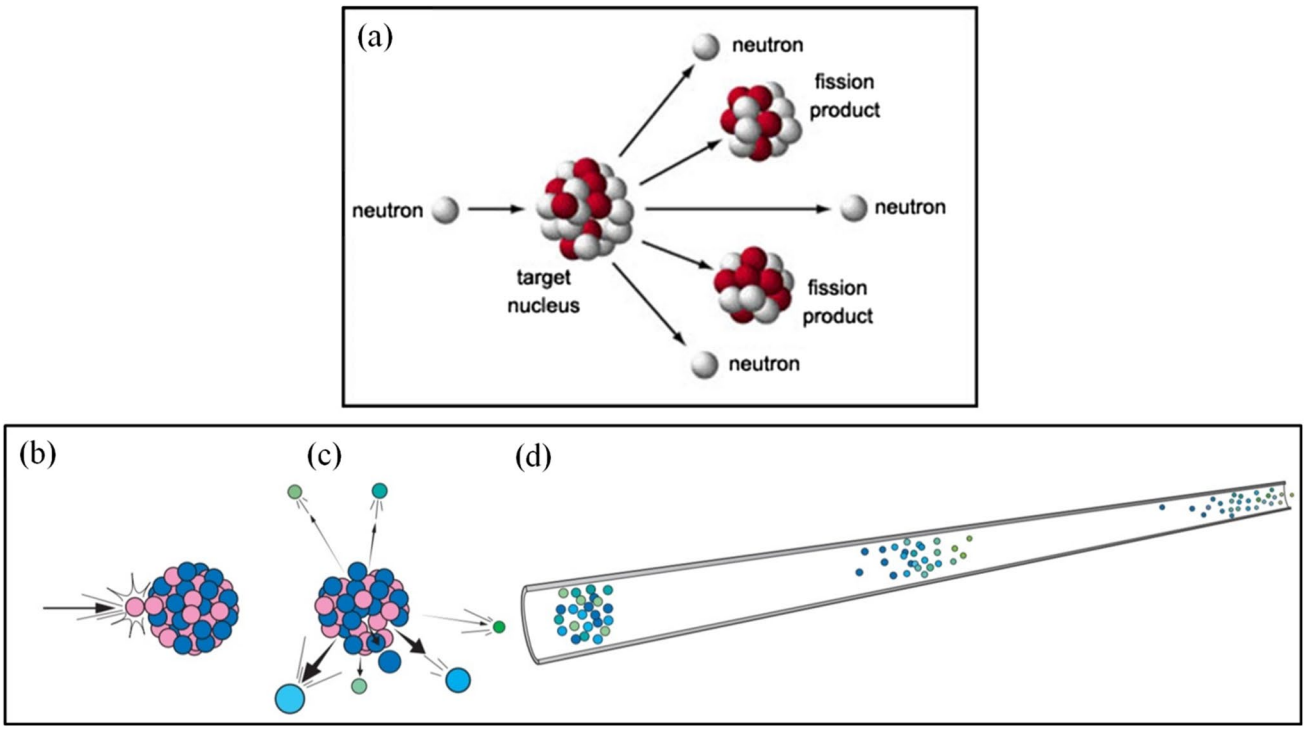

Fig. 7 The fission process (**a**) and spallation process showing the collision of pulse energetic protons (pink) with a tungsten nucleus (**b**) which causes the nucleus to release neutrons at different energy levels as shown by different colors (**c**) and neutrons traveling in specific direction along a beamline (**d**) [48, 49]

[17, 50]. The constructive interference occurs at specific scattering angles (2θ) where the path length difference of two incident neutron beams is an integer multiple of the wavelengths [47, 51], as described by Bragg's Law and illustrated in Figure 8.

The d-spacing (lattice spacing) can then be measured in the perpendicular direction to the lattice planes in a scattering volume, in the direction of the scattering vector, as shown in Figure 9. Figure 10 shows the positioning of the engine block to allow the scattering vector to be in the radial direction relative to the cylinder bore (d-spacing measurement in the radial direction of the engine block). As mentioned earlier, nuclear research reactors utilize a continuous monochromatic neutron beam with a fixed and known wavelength. ND measurement gives the d-spacing d_{hkl} changes as a function of $2\theta_{hkl}$ (Eq. (2)). Despite similarities in the fundamental principles of the X-ray and other diffraction techniques, neutron diffraction has the unique advantage of being able to penetrate several centimeters through the thickness of most of the alloys and metals (by interacting with the atomic nuclei rather than the electron cloud [51]), enabling stress measurements in the bulk of the components to a depth of 5 cm or more in Al-Si alloy part of the engine block.

For a pulsed neutron beam (white beam from a spallation source), the diffraction angle $2\theta_{hkl}$ is fixed, and the beam wavelength is determined based on the traveling distance and the arrival time (t) of neutrons at the detectors. Figure 9b shows the TOF technique, which utilizes the elapsed time (t) for the neutron beam traveling from a source to a detector. As a result, the distinct peaks can be measured in a whole range of d-spacings and separate responses of each (hkl) orientation among grains with their plane normal parallel to the diffraction vector Q (Figure 9b). By utilizing the least squares Gaussian fitting method (Figure 11a), the single peak (d_{hkl}) of the continuous beam diffraction can be obtained from a reactor based

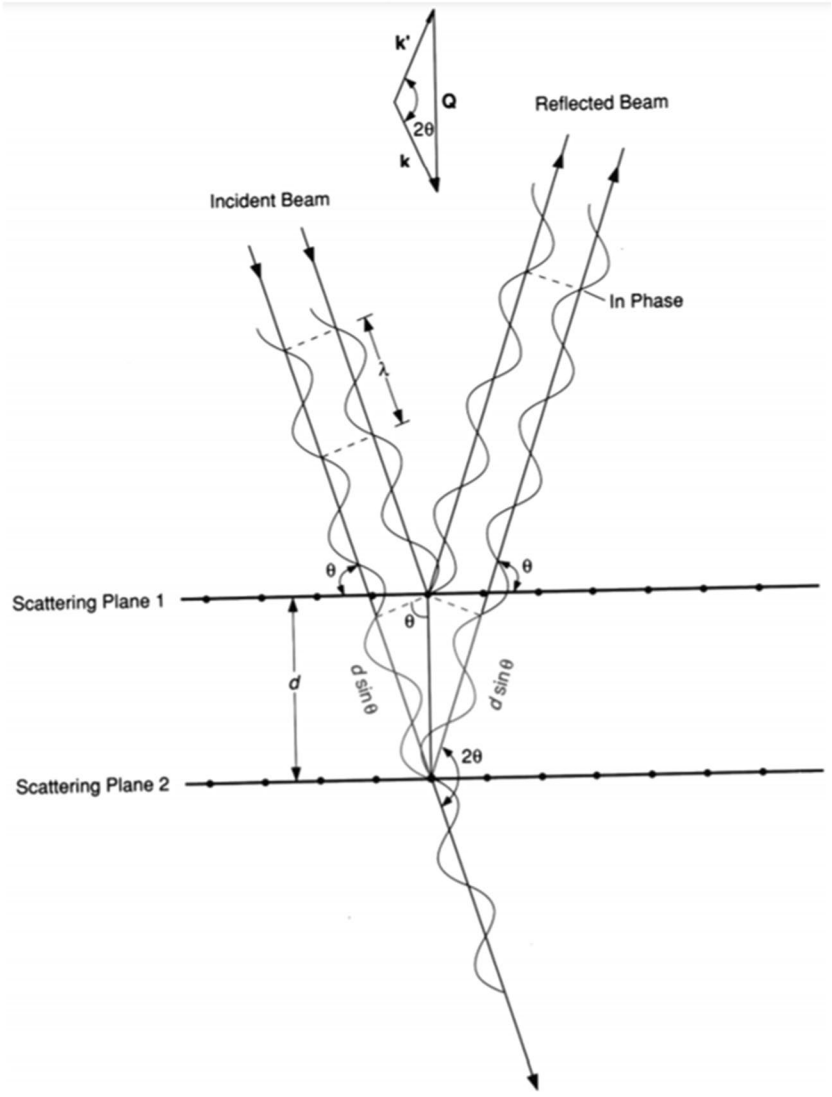

Fig. 8 Constructive interference occurs when the path length difference of two incident neutron beams from adjacent scattering planes are in phase with each other, and the path length difference of diffracted rays is an integer multiple of the wavelength. The figure shows the extra distance traveled by the wave scattered from the Scattering Plane 2, which is defined by the Bragg Law [52]

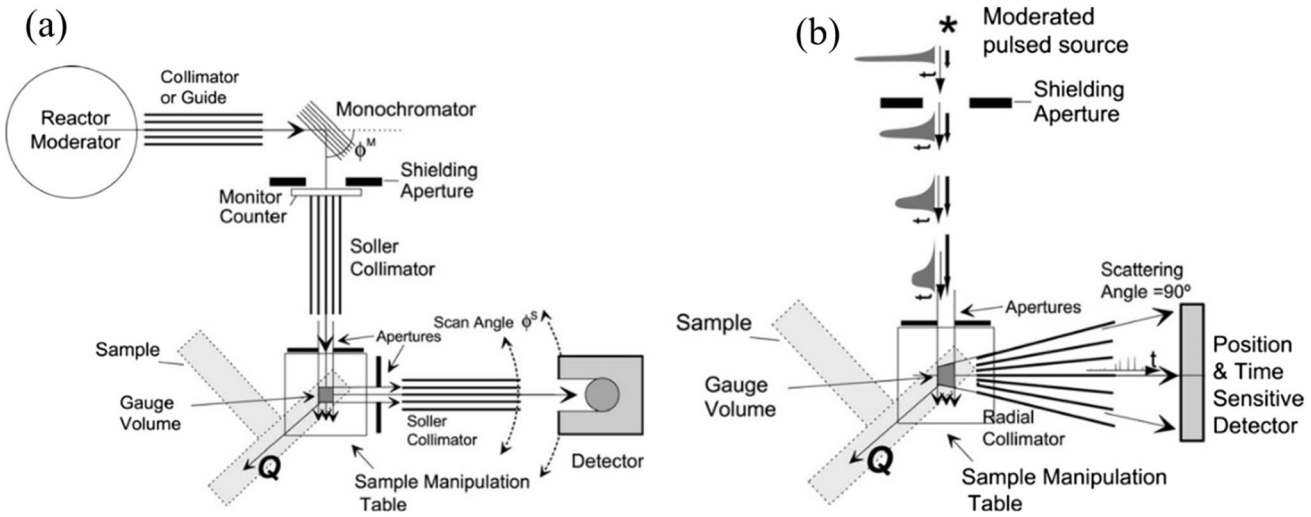

Fig. 9 Schematic of a reactor-based (constant flux) neutron diffraction spectrometer and (b) time-of-flight instrument at the spallation neutron source [53]

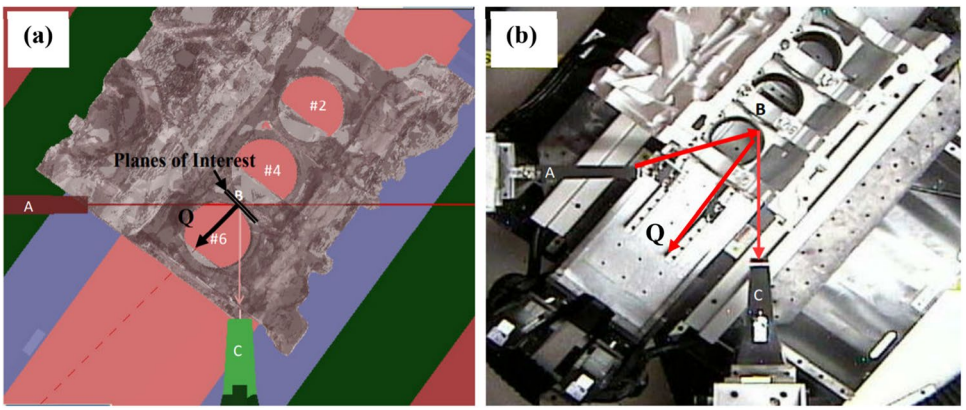

Fig. 10 Orientation of incident (A) and scattering beam (B) in the measurement of residual strain in the direction of scattering vector (Q) in engine block; **a** virtual model of the sample and test simulation and **b** actual positioning of the engine block on the sample table [54]

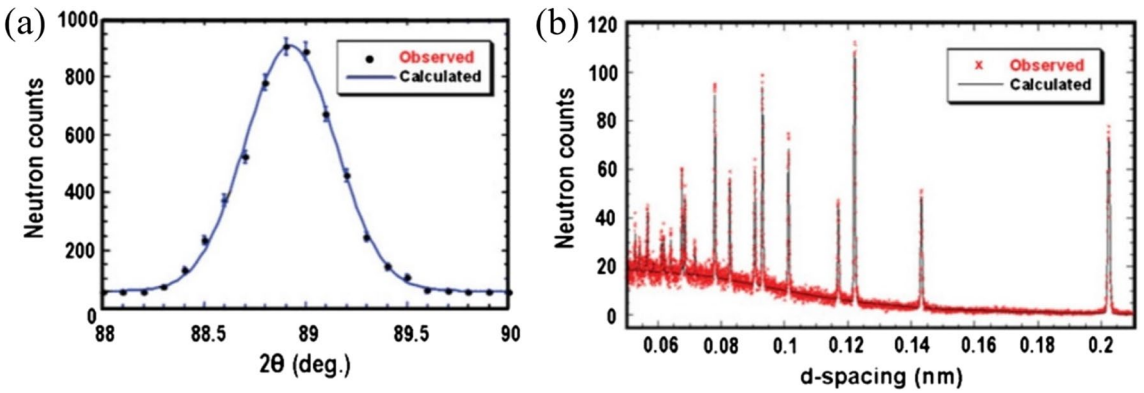

Fig. 11 Example of **a** Gaussian distribution fitted for the brag peak from reactor-based diffractometer and **b** diffraction spectrum pulsed neutron beam fitted with Rietveld refinements [45, 46]

instrument, while Rietveld refinement method is used to analyze the full peak pattern of the pulsed neutron beam, which is diffracted from various crystallographic lattice planes in a particular material direction. Figure 11b shows a typical diffraction spectrum from a pulsed neutron beam instrument and the result of a Rietveld profile analysis.

By using the "peak shift" method, the lattice strain can be calculated by measuring lattice spacing for both stressed sample (d_{hkl}) and stress-free or unstrained sample ($d_{hkl,0}$) of the same chemical composition (Eq. 3).

$$\varepsilon_{hkl} = \frac{d_{hkl} - d_{hkl,0}}{d_{hkl,0}} \tag{3}$$

The generalized Hooke's law (Eq. 4) is then utilized to convert three orientations of elastic strain (i.e., ε_R, ε_A, ε_H) into principal residual stresses ($\sigma_R, \sigma_H, \sigma_A$)

$$\sigma_{R,H,A} = \frac{E}{1+\upsilon}\left[\varepsilon_{R,H,A} + \frac{v}{1-2v}\left(\varepsilon_R + \varepsilon_A + \varepsilon_H\right)\right] \tag{4}$$

2.2.3 Applications of neutron diffraction in residual stress measurements for engine blocks

Neutron diffraction has been utilized extensively for the characterization of the residual stresses at different steps during the manufacturing process (i.e., as-cast, heat-treated, etc.) of engine blocks.

A study conducted by Sediako et al. [43, 55] utilized ND to characterize the residual stress in the cylinder web region for a sand-cast V6 Al-Si alloy engine block manufactured with gray cast iron liners with flake graphite. The results indicated that a high magnitude of tensile residual stresses was present in both the gray cast iron liners (~180 MPa) and Al-Si alloy (~200 MPa, higher than the yield strength of Al). Microstructural analysis revealed some variations in the cooling rate along the cylinder depth. A higher cooling rate was observed at the bottom of the cylinder, compared with the top, which led to a more refined grain structure (refinement of Al_2Cu, $Al_{15}(Mn,Fe)3Si_2$, and eutectic silicon) as well as more globular and uniform distribution of second-phase particles resulting in increased hardness for this region. The result obtained by neutron diffraction was in agreement with the hardness and microstructural analysis, where a lower magnitude of residual stress in all directions was observed at the top of the cylinder corresponding to the lower cooling rate and coarsened microstructure. The residual stresses measured in [43] led to the conclusion that the stresses may induce permanent dimensional distortion in the engine block, which is detrimental to the engine operating

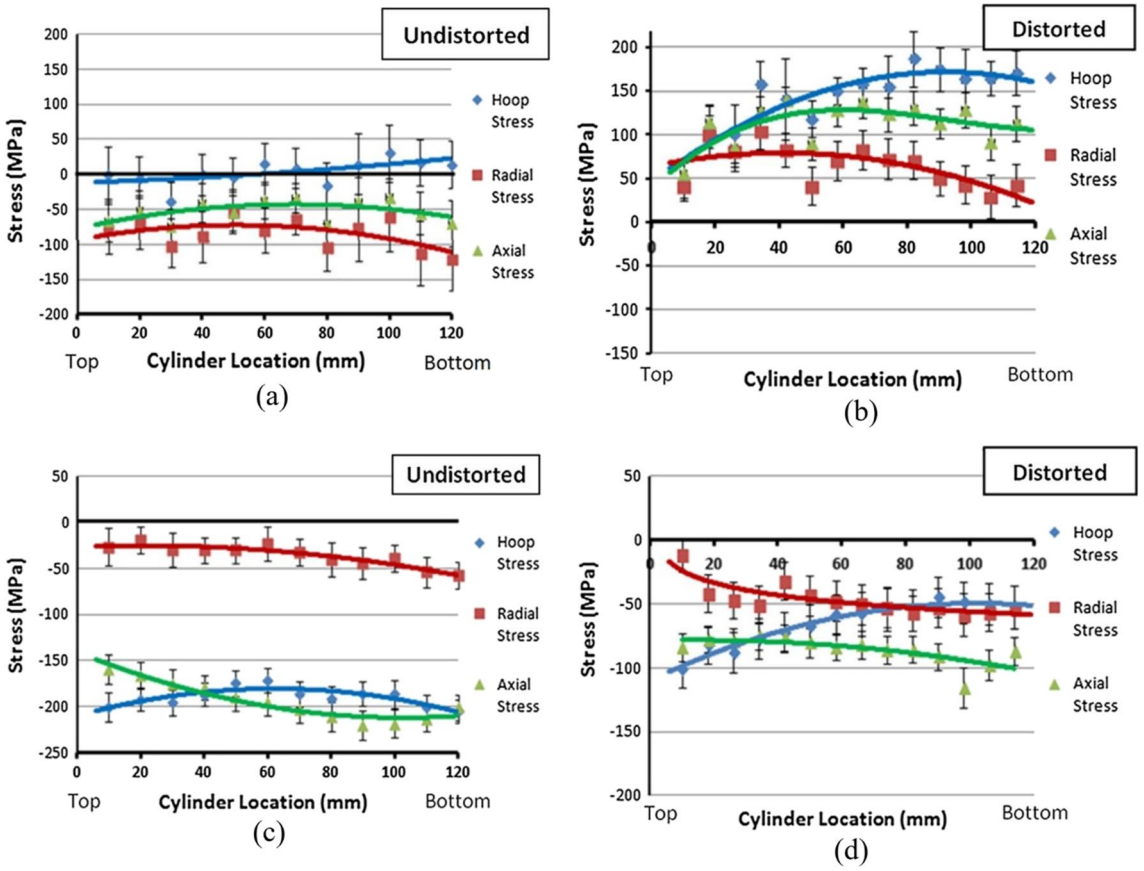

Fig. 12 Residual stress profiles for the aluminum cylinder bridge (**a**, **b**) and gray cast iron cylinder liners (**c**, **d**) of the undistorted and distorted engine block [56]

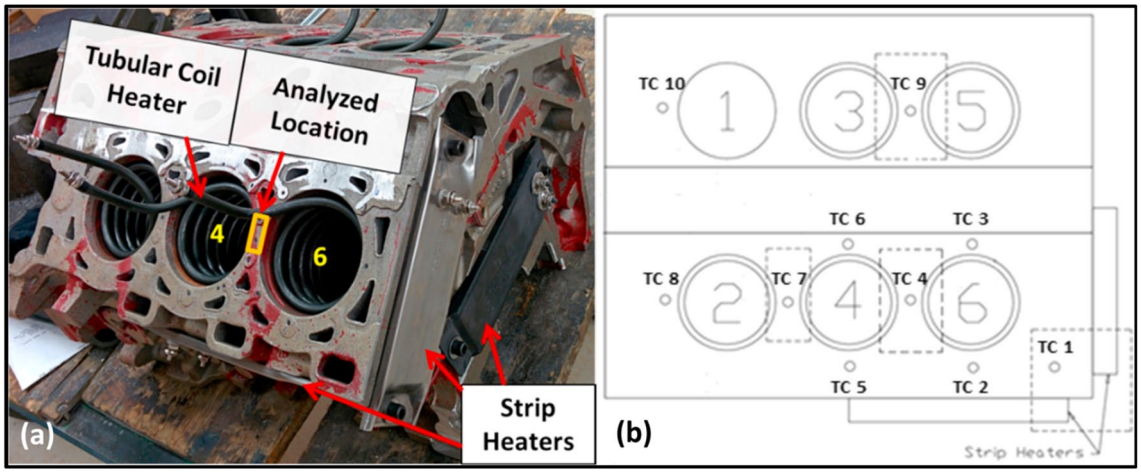

Fig. 13 Experimental setup including **a** coil and strip heaters used for heat treatment of the engine blocks, **b** sketch of thermocouple locations for monitoring engine temperature during heat treatment [36]

efficiency, increased carbon emission, and high operation cost (i.e., extensive and expensive recalls) in consequences.

Lombardi et al. [56] carried out a comprehensive investigation, including residual stress, mechanical properties, and microstructure characterization for distorted and undistorted cast Al-Si alloy engine blocks to identify the cause of distortion along the cylinder bores. A high tensile residual stress was found in the Al-Si alloy in the distorted engine block, particularly in the hoop direction, with a magnitude of 170 MPa (Figure 12b). The magnitude of tensile residual stress accounts for more than 80% of the alloy's available strength, and once in service, the operating conditions superimpose on the existing stresses, and the engine block may endure permanent dimensional distortion or cracking. This distortion or cracking can result in reduced engine efficiency, increased carbon emission, and/or complete engine break down.

Furthermore, non-uniform distortion was found in the distorted engine block, which was associated with the differential cooling rates, shown by microstructural changes in the cylinder (coarse and fine microstructure was found from top to bottom of the cylinder). For instance, the low magnitude of distortion measured at the top of the cylinder (the region with coarse microstructures and lower strength) was caused by lower residual stresses in all three directions, which prevents plastic deformation and minimizes creep deformation during service. Both the distorted and undistorted engine blocks contained coarse primary Al dendrites and secondary phase particles (eutectic Si, $Al_{17}(Fe,Mn)_4Si_2$, $Al_5Mg_8Cu_2Si_6$, and Al_2Cu) at the top of the cylinder, while the bottom of the cylinder contained significantly refined Al dendrites and secondary phase particles. Furthermore, there were no differences in shape, size, and distribution of the volume fraction of the secondary phase, which contained fully stabilized

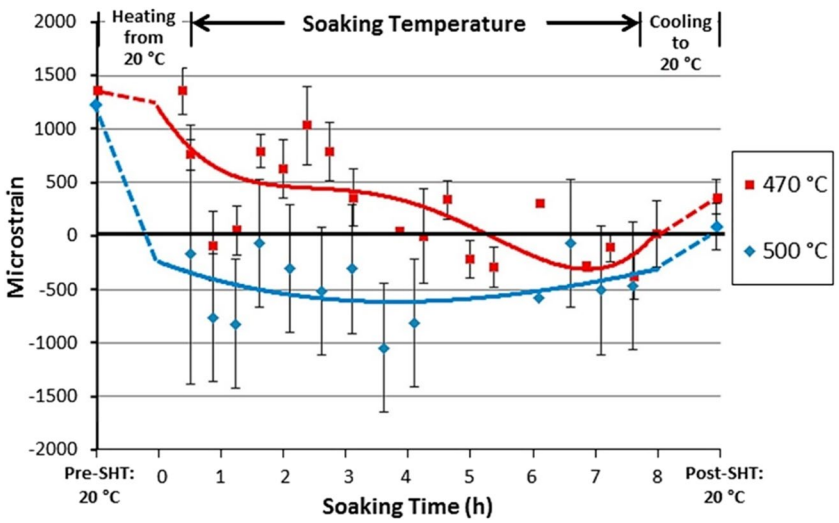

Fig. 14 In situ residual strain relaxation in the axial direction during solution heat treatment of Al-Si alloy engine blocks [36]

h-Al_2Cu age-hardening precipitates. The thermally stable microstructure indicated that distortion was not caused by thermal grain growth.

A relatively constant residual stress profile for the undistorted block was found with the highly compressive residual stresses in the axial and radial orientations (Figure 12a). The compressive axial stress in the undistorted engine block varied between 50 and 70 MPa along the cylinder bridge while the radial stress varied between 80 and 120 MPa. In the hoop direction, in contrast, compressive residual stress was found near the top of the cylinder with a magnitude of approximately 10 MPa which gradually becomes tensile near the bottom of the cylinder bridge with the magnitude of approximately 20 MPa. Similarly, the compressive residual stresses were found along the gray cast iron liners of both undistorted and distorted engine blocks. In the undistorted engine block, the compressive stress in the axial direction varied from 150 MPa near the top to approximately 210 MPa near the bottom of the cylinder liner. Compressive hoop stress with a magnitude of approximately 175 MPa was found in the middle of the cylinder while the top and bottom of the cylinder experienced a magnitude of 200 MPa.

The residual stresses were compressive along the gray cast iron liners of the distorted and undistorted engine blocks (Figure 12 c and d). The undistorted engine block had a compressive radial stress that was 30 MPa at the top of the cylinder and gradually increased to 50 MPa at the bottom of the cylinder. In addition, the axial stress varied from 150 MPa near the top of the cylinder liner to approximately 210 MPa near the bottom. Similarly, the compressive hoop stress had a magnitude of 200 MPa near the top and bottom of the cylinder, while the middle of the cylinder had a magnitude of approximately 175 MPa.

Different post-processing techniques, such as solution heat treatment (SHT) and artificial aging, were utilized to mitigate the high tensile residual stresses in the engine blocks [57, 58]. The use of neutron diffraction to measure residual stresses prior to, during, and after heat treatment of the engine blocks was the subject of several experimental studies.

Lombardi et al. [23, 36] utilized in situ ND to evaluate the relaxation of residual strains in the cylinder bridge as a function of time during SHT. Ex situ ND was also performed to evaluate residual stresses before and after solution heat treatment. In addition, the stress-free interplanar spacing (d0) was also measured as a function of time during heat treatment to correct for thermal expansion and phase dissolution. The engine blocks the production T4 heat treatment (SHT at 470 °C for 7.5 h, followed by forced air cooling) were also analyzed to investigate the thermal gradient effects induced by air quenching on the residual stress profiles.

They designed a unique heating system including coiled tubular heaters in the bore cylinders and strip heaters in the front and side of the engine block, as shown in Figure 13.

The study used a monochromatic neutron beam with a wavelength of 1.55 Å. For the *in situ* ND experiments, the Al (331) planes (axial direction only due to equipment constraints) were used. In comparison, two different planes of the Al (311) (hoop direction) and (331) (axial and radial directions) were used for the ex situ experiments. Gradual relief of tensile residual strain occurred during SHT at 470 °C with the complete strain relaxation happening up to approximately 5 h of soaking time; at 500 °C, complete relief of tensile residual strain occurred in just under 0.5 h, as shown in Figure 14. The results indicated that dislocation creep is responsible for strain relaxation during SHT. Ex situ ND was also conducted before and after the SHT, which showed a significant reduction of tensile residual stress as well as uniformity in the stress magnitudes in the cylinder bridge in all three orientations (hoop, axial, and radial directions), as can be seen in Figure 15. The authors also investigated the effect of production T4 treatment on the engine block (470 °C for 7.5 h, forced air quench). There were significant variations in the magnitude of residual stresses along the cylinder bridge due to forced air quench and resultant thermal gradients,

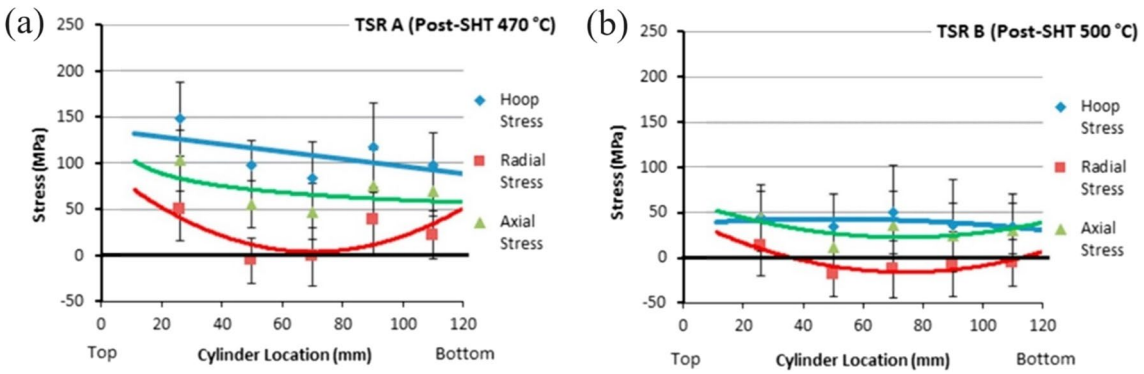

Fig. 15 Ex situ residual stress profiles for the engine blocks following SHT at **a** 470 °C, **b** 500 °C [36]

which promoted more stress development in specific locations of the CB. In another study conducted by Lombardi et al. [59], it was found that high residual stresses in the cylinder bridges of a sand-cast V6 Al-Si-Cu alloy (A319 alloy) engine block were reduced considerably after a T7 heat treatment. It was noted that the T7 heat treatment led to substantial stress relief at the top of the cylinder in the Al-Si-Cu alloy part of CB. In contrast, the middle and bottom regions experienced only minor changes. This could be associated with non-uniform cooling throughout the cylinder bore following solution treatment. It was also found that the over-aging (T7) treatment caused a redistribution of the tensile residual stress from the top of the cylinder to the bottom. It was also observed that lower-strength sections (large grain structure) are more prone to stress relief and distortion than higher-strength parts (fine grain structure) [43, 59–61].

Neutron diffraction–based residual stress measurements were applied to sand-cast A319 engine blocks subjected to T5 heat treatment, as reported by [62]. The results indicated that T5 was less effective in relieving the tensile residual stresses than the T4 treatment. This outcome is likely to be due to the lower aging temperature for the T5 treatment (255 °C) in comparison with the solutionizing temperature of the T4 treatment (470 °C), as stress relief during heat treatment is highly dependent on the specimen temperature, as reported in previous studies of [23, 58, 63].

Liu et al. [64, 65] studied the evolution of residual strains along the cylinder bridge of A383 high-pressure die casting (HPDC) V6 engine blocks, as shown in Figure 16. The strains were only measured in the hoop and axial directions in the Al-Si alloy part of the cylinder bridge and compared the results of as-cast and T5-treated blocks. The authors measured maximum residual stresses of +70 MPa and +46 MPa in the hoop and axial orientations in the as-cast engine block, which was significantly lower in magnitude than the sand-cast A319 engine blocks as reported by Lombardi et al. [36] for sand-cast A319 engine block. They claimed that the T5 heat treatment relaxed the residual strains significantly in the axial direction, while the residual strains in the hoop direction were relaxed only slightly after heat treatment; though these were different casting techniques and engine blocks with different Al-Si alloys. Also, the authors did not study the impact of gray cast iron liner on the evolution of residual stresses in the HPDC engine block, which should lead to high stresses in the Al-Si alloy due to differential thermal expansion during cooling.

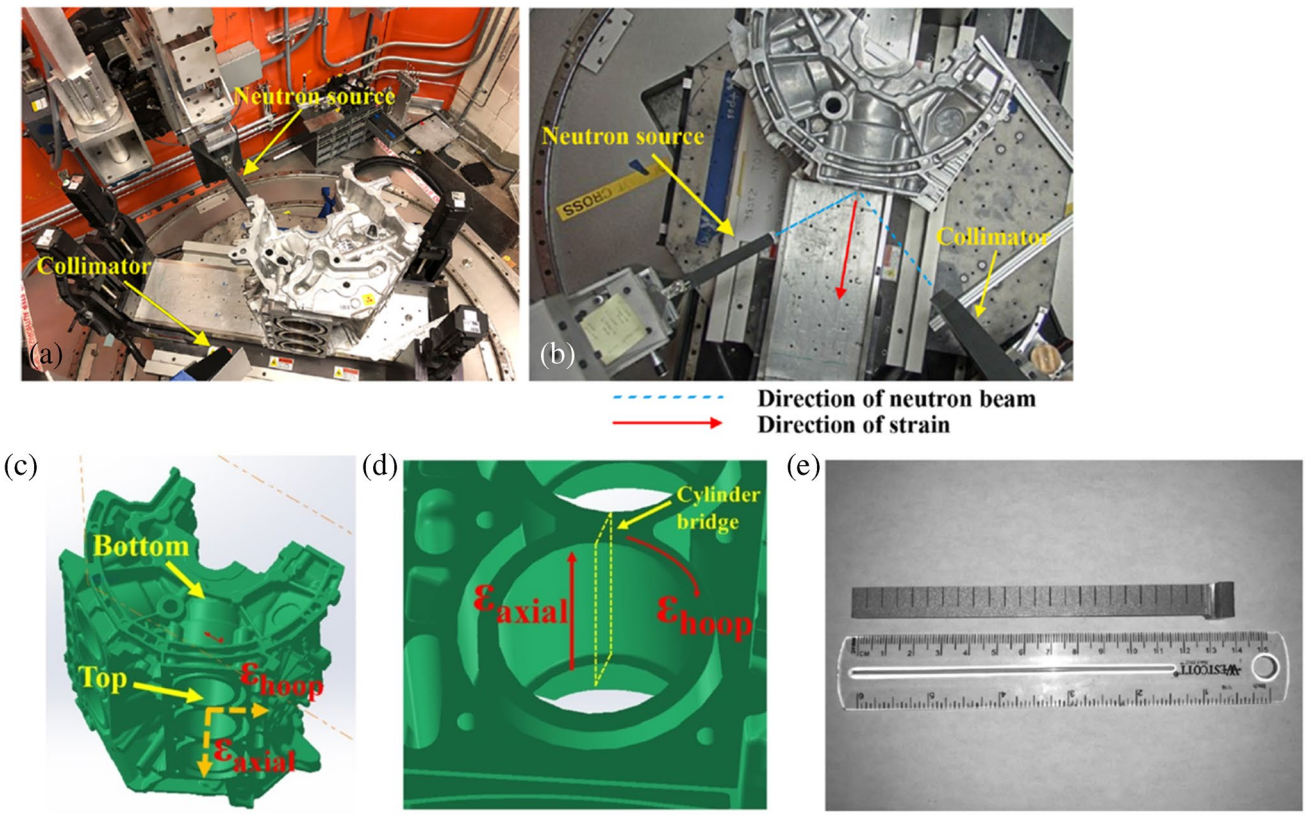

Fig. 16 Experimental setup for ND at NRSF-2; **a** with the strain measurement in the hoop direction, **b** strain measurement in the axial direction, **c** and **d** schematic that shows the geometry of the A383 engine block, **e** strain-free specimen with a "comb" geometry [65]

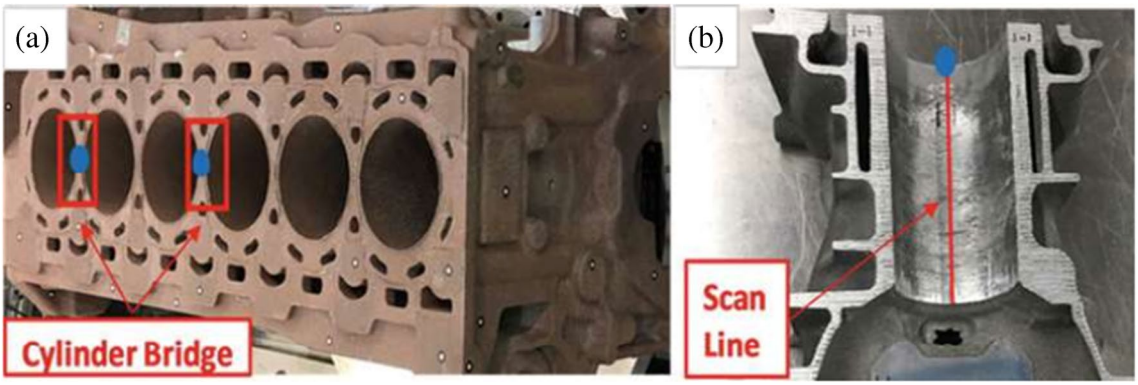

Fig. 17 Location of scan lines [66]

In an effort to study the impacts of casting and heat treatment processes on the residual stress profiles, Stroh et al. [66] applied ex situ ND to a T7 heat-treated precision sand-cast bore-chilled I6 Al-Si alloy engine block. A modified Nemak-Cosworth mold design was used to cast the engine block with a focus on improving microstructural properties (i.e., grain refinement in cylinder bores) and reducing residual stress during casting by removing the gray cast iron liners.

The stress profiles in two of the five-cylinder bridges were measured, as shown in Fig. 17a, to determine the uniformity of the residual stress magnitude and profiles throughout the engine block (see Figure 17).

It was concluded that removing the gray cast iron liners from the casting process significantly reduced residual stress in Al-Si alloy engine blocks (this leaves the option of inserting liners later with less interference fit, or using a steel or ceramic coating directly on the Al-Si block). This residual

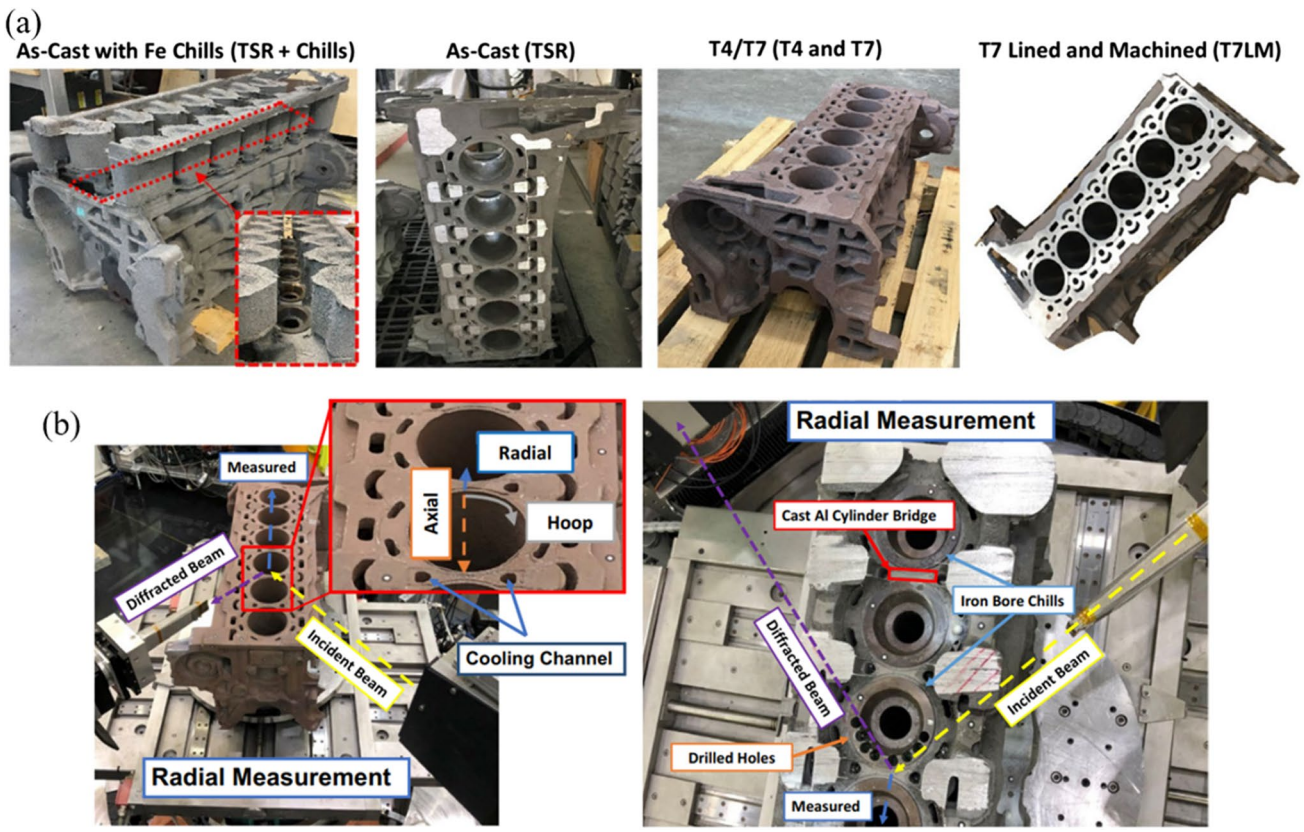

Fig. 18 **a** Engine blocks used for the experiments; and **b** ND experimental setup at the Kowari strain scanner (Sydney, Australia) [67]

Table 1 Summary of the neutron diffraction residual stress measurements in various engine blocks

Type of engine block	Instrument/facility	Manufacturing process	Maximum RS, MPa	Stress component	Authors (references)
Inline 6-cylinder (319 Al alloy)	KOWARI/ANSTO Australia	T4 heat treatment (Cylinder Bridge) T7 heat treatment (Cylinder Bridge) T7 heat treatment-production ready with the pressed cast iron liners	+150 +120 +61	Axial Axial Axial	Stroh et al. [67]
V 6 (319 Al alloy)	CNBC/Chalk Rivers Canada	TSR (Cylinder Bridge) T7 heat treatment (Cylinder Bridge) Dyno-Tested (Cylinder Bridge) TSR (Gray cast Iron Cylinder Liners) T7 heat treatment (Gray Iron Cylinder Liners)	+195 (TOC) +204 (MOC) +190 +107 +105	Hoop Hoop Hoop Radial Axial	Lombardi et al. [59]
V 6 (319 Al alloy)	CNBC/Chalk Rivers (in-situ and ex-situ ND) Canada	As-cast T4 heat treatment (Cylinder Bridge)	+220 +120	Hoop Hoop	Lombardi et al. [23, 36]
V6 (HDPC Al 383 alloy)	NRSF2/ORNL USA	As-cast (Cylinder Bridge)	+70	Hoop	Liu et al. [64, 65]
V 6 (319 Al alloy)	CNBC/Chalk Rivers Canada	As-cast (Cylinder Web-Al-Si) As-cast (Cylinder Web-Gay Cast Iron liners)	+200 +180	Hoop Hoop	Sediako et al. [43, 55]
V 6 (319 Al alloy)	Kowari/ANSTO Australia	As-cast (Cylinder Bridge) T7 heat treatment (Cylinder Bridge)	+100 -175	Radial Axial	Stroh et al. [66]

stress drop was partially associated with the reduced restriction of Al-Si alloy contraction during casting's cooling down upon complete solidification. The authors also observed similar stress profiles in the two scanned cylinder bridges, which indicates a uniform cooling rate with a congruent thermal gradient during casting. Finally, T7 heat treatment was successfully applied. It resulted in a significant reduction of residual stress/strain from the CBs, particularly in the radial orientation, where a reduction of residual stress from 100 to 50 MPa was observed at the top of CB (i.e., the location most prone to distortion and cracking) [66]. In another study, Stroh et al. [67] utilized neutron diffraction to investigate the evolution of residual stress for different steps along the manufacturing process of the inline 6-cylinder sand-cast Al-Si alloy engine block with mechanically pressed-in iron cylinder liners. The engine blocks used and the experimental setup for this study are shown in Fig. 18a, b. Utilizing bore chills during the casting process led to the formation of a high magnitude of compressive residual stresses in three orientations of the CB, which was relaxed considerably after the bore chills removal (greater than −300 to ~100 MPa). The stress mode remained partially compressive after T7 heat treatment and with the mechanically inserted iron cylinder liners, which minimized the material's susceptibility to crack growth and propagation. Table 1 summarizes the previous studies of neutron diffraction measurement of residual stresses in the engine block.

Neutron diffraction was able to measure the residual stresses in many locations in engine blocks; the full stress tensor can be calculated. Some sample preparation is required, particularly in thick sections, and a stress-free sample of the same material is required to make a stress-free d-zero sample. To measure different materials generally requires a change of monochromator, wavelength, and instrument geometry, which will increase the experimental time significantly.

3 Numerical methods

3.1 Finite element modelling of residual stresses

Numerical simulation, with experimental validation, at the early stages of design could substantially reduce the associated costs of the trial and error procedure of experimental casting, leading to large decreases in energy and material consumption [40, 68]. It can also speed up the design cycle by predicting casting defects and allowing designers to improve the product's design and quality [69, 70]. Advances in modelling along with faster computing hardware allow the process developer to have a better understanding of the casting process with reasonable accuracy in a short amount of time [71].

3.2 The thermal conditions during casting

FEM requires an accurate temperature field and temperature-dependent material properties; the temperature field is

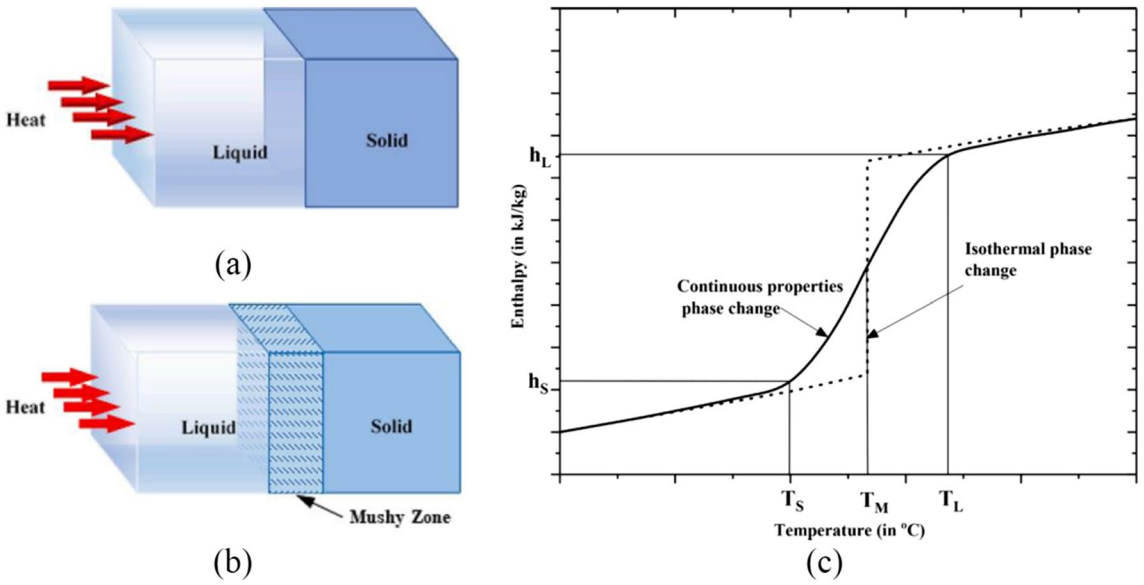

Fig. 19 The schematic view of **a** a pure substance melting and **b** an alloy melting. **c** The changes in enthalpy during solidification of a pure substance (isothermal phase change) and alloy (continues properties phase change) [72]

difficult to measure and model. Metal solidification in casting is very complex and significantly impacts the casting quality, cycle time, and process yield [72]. Solidification is a phase transition process of liquid metal into the solid state, which is accompanied by the release of the material's latent heat. During this process, a boundary between the newly formed solid phase and liquid moves through the material. The boundary for pure metals differs from the one for alloys. While there is a sharp transition from liquid to solid phases in pure metals, the alloys have the solidification phase change in the form of a mushy zone, as shown in Figure 19 a and b. In other words, the phase change in pure metals happens at a single temperature, i.e., melting temperature (TM), and in alloys, it occurs in a range of temperatures, i.e., between liquidus (TL) and solidus (TS), as shown in Figure 19c.

The thermal field models of the solidification process are mainly of two different types [73]. In the first category, two different media are defined for the liquid and solid phases. Consequently, continuity equations, including heat flow and temperature, are solved separately for each medium and their interface. These two-domain approaches, also called "front tracking," are normally utilized for modelling the solidification of pure materials. In the second approach, a single medium/domain is applied to both liquid and solid phases, and average quantities, such as solid fraction and enthalpy, are defined at the nodes of the domain. Therefore, due to the definition of average quantities in the domain, these methods show a better capability to model alloy solidification, which happens by forming a mushy zone in a temperature range [73]. Most commercial FE packages use the second method to model the thermal field of material solidification [74].

The numerical simulation of the solidification process is challenging due to several factors including the nonlinear transient nature of the solidification mechanism, heat and mass transfer occurrence at microscopic and macroscopic scales, microstructure development, and the major impacts of fluid flow on solidification. Residual stress is inevitable in casting, which may lead to dimensional distortion or failure of cast components.

The prediction of the residual stress in early design steps can significantly improve the durability and efficiency of the cast parts and reducing their production costs [10]. In

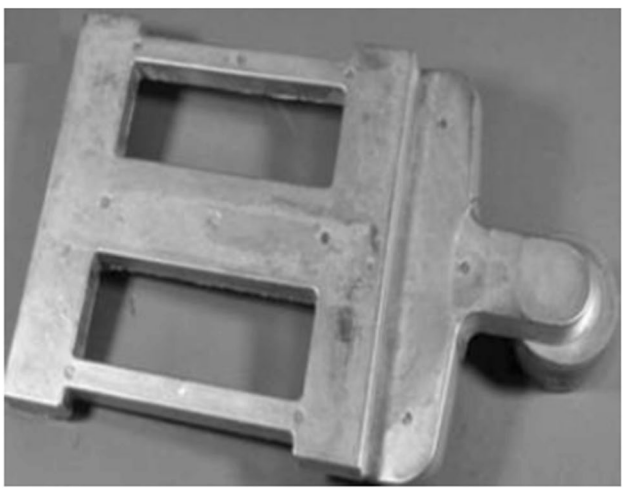

Fig. 20 The HPDC stress-lattice specimen [79]

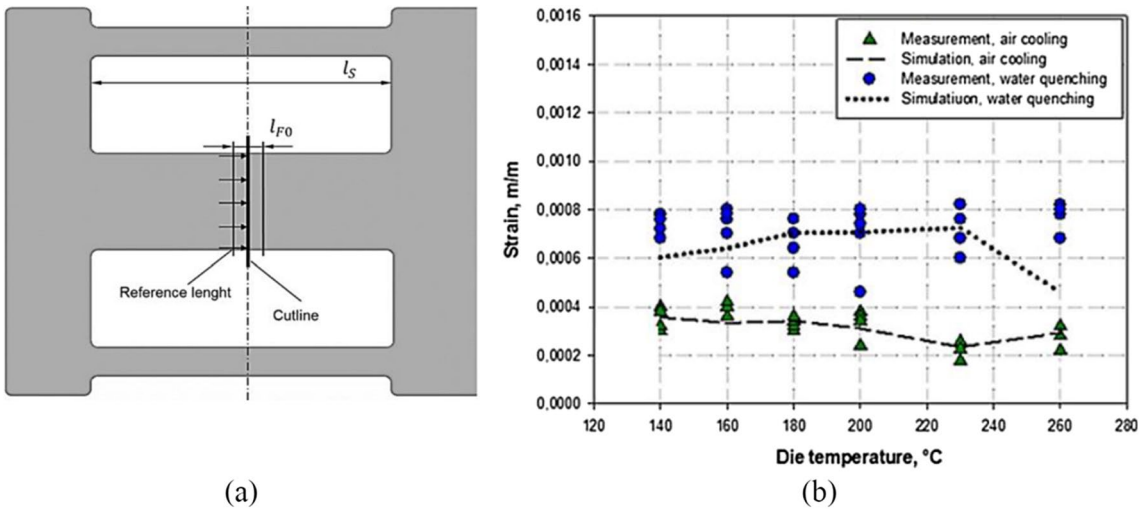

Fig. 21 **a** Evaluation of the strain and elongation in the stress-lattice, **b** comparison of numerical simulation and experimental measurement of the calculated elastic strains in the stress-lattice's middle arm [78]

particular, understanding the residual stress development via modelling is even more crucial for cast components with complex geometries, such as engine blocks, due to the time-consuming and costly prototyping.

Prediction of residual stress via FEM during solidification is done through coupled and uncoupled thermo-mechanical analyses. In the coupled method, the thermomechanical contact model is considered in the simulation process [68]; this is only significant where the casting process changes the thermal history. In the uncoupled analysis, the temperature analysis is first conducted from the solidification calculation, and then the temperature history is considered to be a boundary condition to calculate stresses in the mechanical model [75]. Despite the more accurate results of the coupled approach, it is significantly longer compared to its uncoupled counterpart. As a result, researchers frequently use the uncoupled technique, which heavily relies on the heat transfer coefficient (HTC) parameter, to simulate the formation of residual stresses during the solidification process [76, 77].

3.3 Benchmark studies on residual stress modelling

FEM is an effective technique for the prediction of residual stresses in the design stage and prior to the production of powertrain cast components like engine blocks. However, engine blocks have large and complex geometries, resulting in time-consuming FEM modelling of the solidification and heat treatment processes. Therefore, it is not efficient to model an entire engine block to develop the FEM analysis techniques and check that the material properties and thermal history inputs are correct. Hence, standard geometries have been used by researchers in order to develop FEM analysis techniques and compare predicted and measured residual stresses. The next section reviews some of the

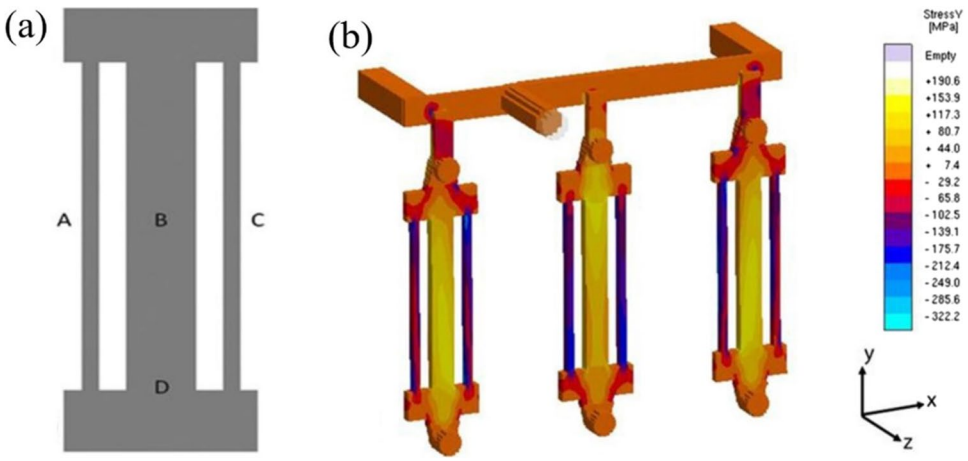

Fig. 22 **a** The casting geometry and the stress measurement locations; **b** stress distribution in the specimen's Y direction [10]

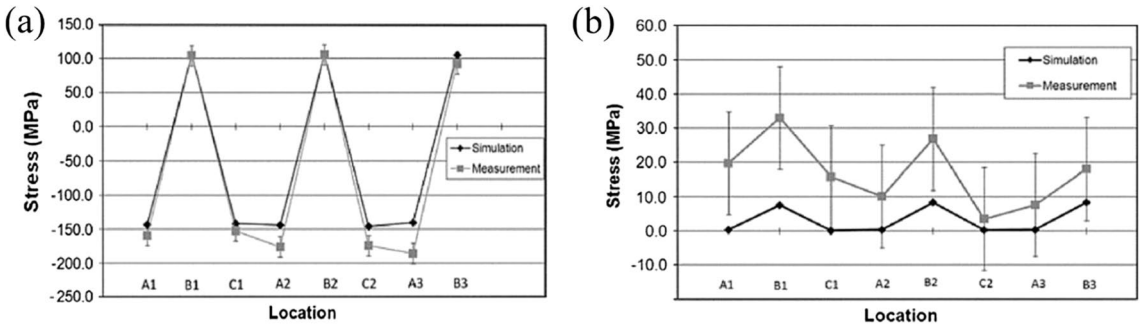

Fig. 23 The comparison between the simulated and measured residual stresses at the specified locations of A, B, and C for the three samples in the **a** longitudinal (Y) and **b** transverse (X) directions [10]

studies that employed a standard geometry to benchmark finite element methods when modelling residual stress in the solidification process.

The stress-lattice geometry is an established method to generate residual stresses in casting components, as shown in Figure 20. This geometry is intentionally designed to generate uneven thermal gradients during solidification and cooling processes via using side (thin) and middle (thick) arms, resulting in residual stress generation in the component without crack formation [10]. It is also a well-established experimental setup for evaluating FEM methodologies [10, 75], which can then be used to analyze more complex geometries such as engine blocks.

Hofer et al. [78] conducted experimentally validated numerical modelling of a stress-lattice casting to investigate the effects of the cooling regime, ejection time, and die temperature on the distortion and residual stress distribution. The HPDC process was utilized to produce Al cast components. The thermal history was obtained through an infrared camera system and used as thermal boundary conditions in ANSYS for the stress analysis. The stress-lattice configuration and comparative analysis between the predicted and measured strains in the stress-lattice's middle arm are shown in Figure 21.

Johnson et al. [10] utilized the MAGMAstress package to investigate the development of residual stresses during the casting process for the gray cast iron stress-lattice specimen. They used the thermo-elasto-plastic material model with temperature-dependent thermo-physical properties in their simulation. The simulation results were compared and validated with the neutron diffraction technique at different locations at the center and side arms (A, B, C, and D). The casting geometry and residual stress profile, in the Y direction, are shown in Figure 22.

Figure 23 shows the comparison between simulation and experimental results. Compressive stresses in the longitudinal direction (Y) of the side arms for all three specimens can be seen while the middle arms were under tensile residual stress. The stress generation mechanism after filling the mold and during solidification and subsequent cooling process of the stress-lattice casting is as follows: due to the difference in the thickness of the side and middle arms, the side arm cools faster than the middle arm, resulting in a lower temperature and, thus, more thermal

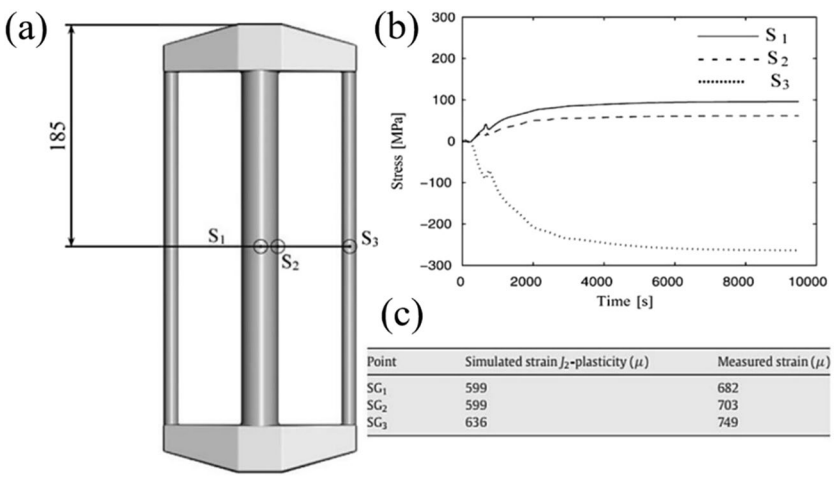

Point	Simulated strain J_2-plasticity (μ)	Measured strain (μ)
SG_1	599	682
SG_2	599	703
SG_3	636	749

Fig. 24 **a** Stress-lattice configuration with the strain gauge locations (S1, S2, and S3), **b** evolution of residual stress as a function of time for S1 to S3. **c** Strain comparison between the numerical model and the experimental measurement (strain relief due to cutting) [75]

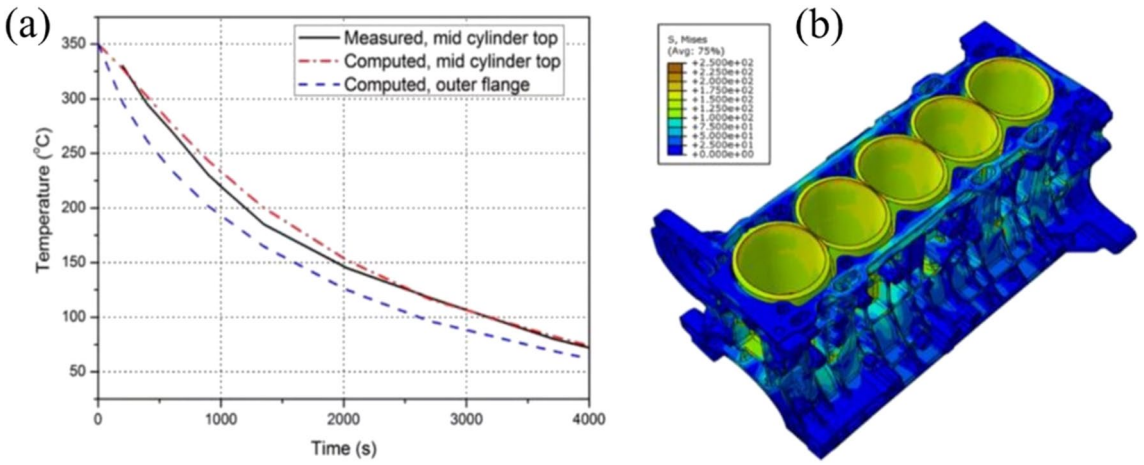

Fig. 25 **a** The cooling curves under convection; **b** the von-Mises stress in the Al-Si alloy block before the machining process [83]

shrinkage of the side arm. This results in the generation of tensile strains in the side arms and compression stresses in the middle arm. When tensile stresses in the side arms surpass their elastic limit, they expand plastically. Following cooling to room temperature, the middle arm is shorter than the side arms, resulting in the generation of compression stresses in the side arms and tension in the middle arm [10, 78].

In a similar study conducted by Gustafsson et al. [75] on a low-alloy gray cast iron stress-lattice, an experimentally validated numerical model (uncoupled thermo-mechanical model) was developed in ABAQUS to simulate the solidification process. The experimental validation was done through the data derived from strain gauges installed at various locations (S1, S2, and S3), as shown in Figure 24a. Two of the strain gauges were mounted in the center of the middle and side arms (S1 and S3), while S2 was installed on the middle arm's surface. Simulation results with the evolution of residual stresses at the selected locations are shown in Figure 24b. There is also some difference in the residual stress (final state) in S1 and S2 which is an indication of the existing stress gradient in the cross-section of the middle arm.

Evolution of residual stress in the gray cast iron stress-lattice was modelled by Motoyama et al. [79, 80]. They validated the FEM results with the sectioning

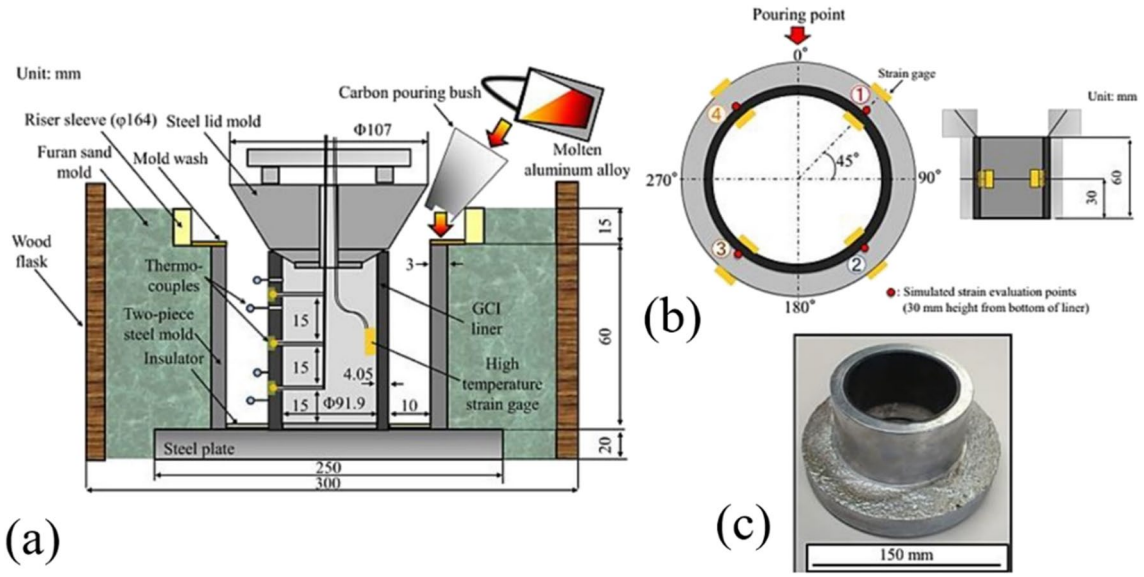

Fig. 26 The casting mold schematic diagram used for the cylindrical shape casting (**a**); the locations of strain gauges for the residual stress measurements (**b**) and the final product with the cast-in iron liner (**c**) [83]

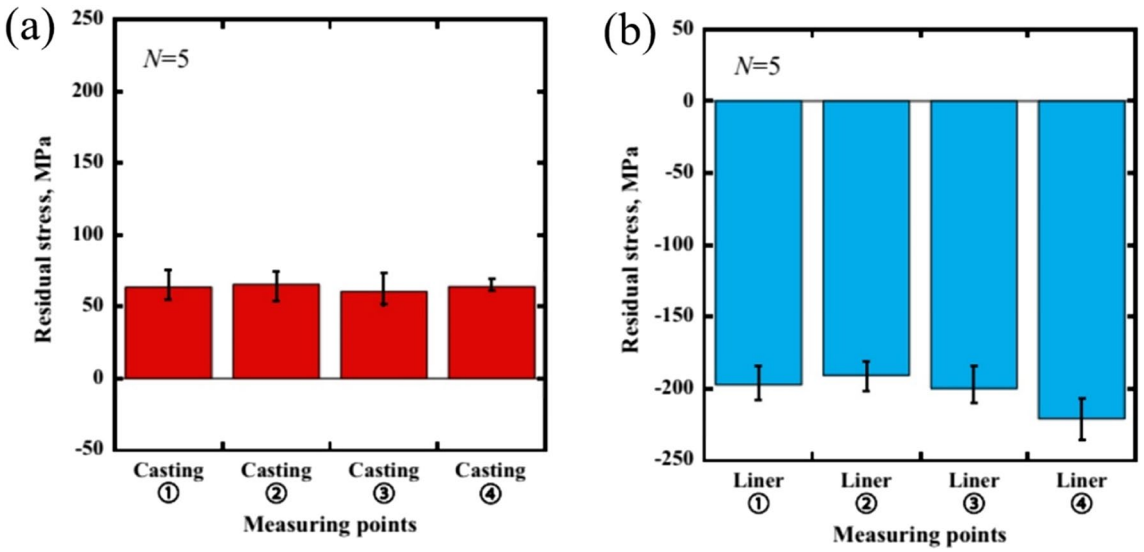

Fig. 27 Residual stresses measured in the circumference direction: **a** Al casting and **b** gray cast iron liner [84]

technique in two orientations of the middle arm (axial and radial). A significant difference between the predicted and measured residual stresses was found in the radial direction, where the modelling results showed significantly higher residual stresses which is an indication that the standard elastoplastic material model overestimates the residual stress. The authors, therefore, introduced a parameter called zero strength temperature (ZST) to the model for the loss of casting's deformation resistance at elevated temperatures [79, 80]. The yield strength of the material was considered to be very low at the temperatures above ZST. The finding of this study showed that the material's strength at melting temperature must be added to the regular elastoplastic model for the accurate prediction of the residual stresses in the cast components [79, 81].

3.4 Finite element modelling of residual stress evolution during engine block solidification

Ahlstrom et al. [82] conducted a thermal stress analysis to quantify the cylinder dimensional distortion in a Volvo gasoline I5 Al-Si alloy engine block with cast-in gray iron liners. The engine block model was done in ANSA, and residual stress/strain computations were conducted in ABAQUS. The Al-Si alloy's mechanical behavior was characterized

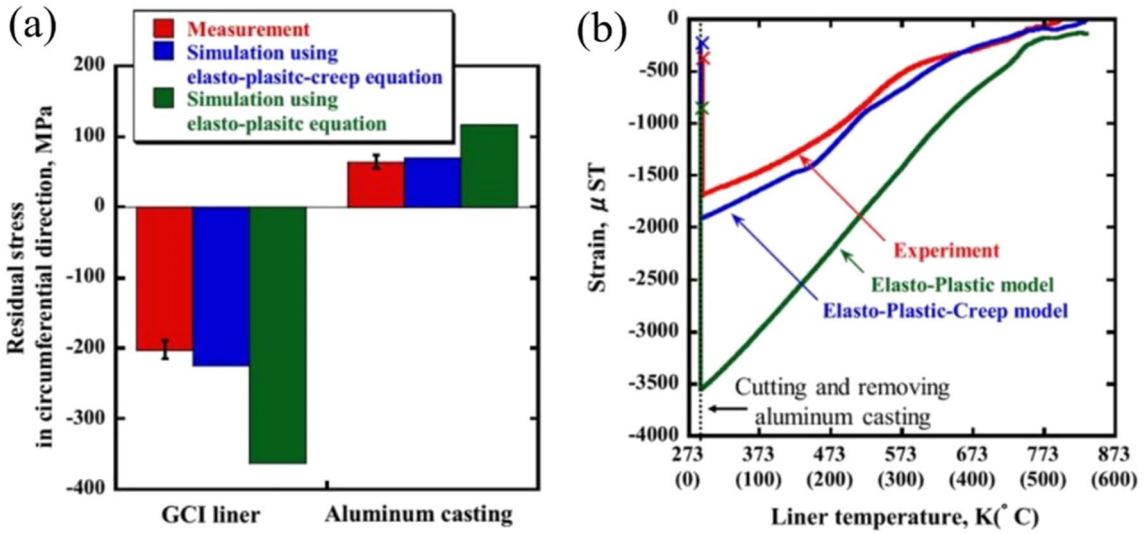

Fig. 28 Comparative analysis between the measured and simulated residual stresses and **a** ex situ and **b** in situ measured stresses in the circumferential orientation [84]

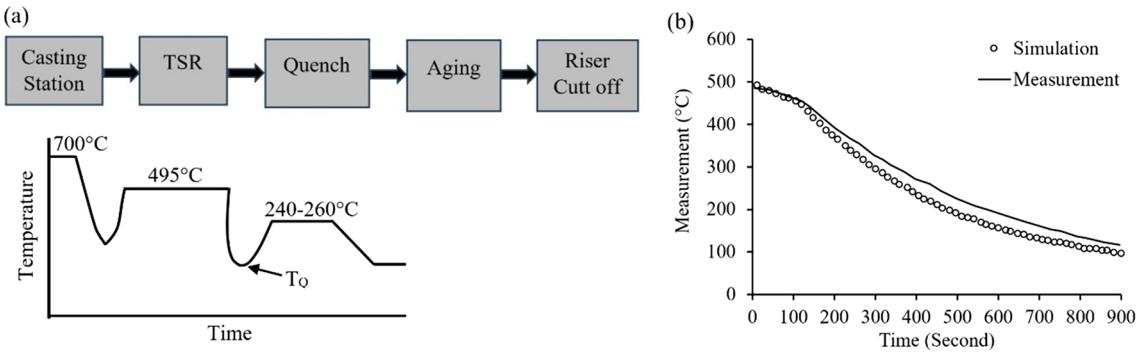

Fig. 29 The analyzed heat treatment process (**a**) and cooling curves (**b**) at the head deck [11]

by tensile tests at different strain rates and temperatures to capture the material's viscoplastic behavior at high temperatures. It is also worth noting that the solidification process (cooling down of the molten metal from liquidus to the solidus temperature) was not considered in the developed model and the simulation started with the ejection of the casting from the mold at 350 to 75 °C (see Figure 25a). This is a simplifying assumption as the non-uniform temperature distribution resulting from the solidification process before 350 °C is not taken into account. The outer surface's heat flux was considered the boundary condition to simulate the block cooling in the air. The distortion introduced by cooling processes was predicted; the out-of-roundness at the top of the cylinder block was in reasonable agreement with the measurements made on a coordinate measuring machine.

Since residual stress formation due to solidification takes place from high to low temperatures, utilizing appropriate material properties at elevated temperatures improves the accuracy of the simulation results. To obtain the accurate results, two important metallurgical phenomena need to be considered: the recovery behavior of the stress-strain curve and the strain-rate dependency. The recovery behavior of materials does not let the inelastic strain formed at elevated temperatures contribute to low-temperature strain hardening. This trend is because, at elevated temperatures, recovery and recrystallization eliminate dislocations and, therefore, minimize the increased dislocation density caused by plastic deformation. Motoyama et al. [83] conducted an experimental and numerical study to determine the circumferential residual stress development in a cylindrical Al-Si-Cu alloy casting equipped with a gray cast iron liner. The experimental setup and the location of installed strain gauges, as well as the final product, are shown in Figure 26. The measured residual stresses in the circumferential direction in the Al-Si-Cu alloy part and gray cast iron liner are shown in Figure 27. There was ~60 MPa tensile residual stress in the Al-Si-Cu alloy part and the gray cast iron liner experienced more than 200 MPa of compressive residual stress in the circumferential orientation. This is expected due to the relative thicknesses of the two materials at this point, with the Al-Si alloy part being thicker.

Motoyama et al. [83] proposed an elastoplastic-creep constitutive model to capture the recovery effect at elevated temperatures and assess its influence on the simulation results. In the FEM model, the coefficient of heat transfer between the metal mold and the casting was achieved by

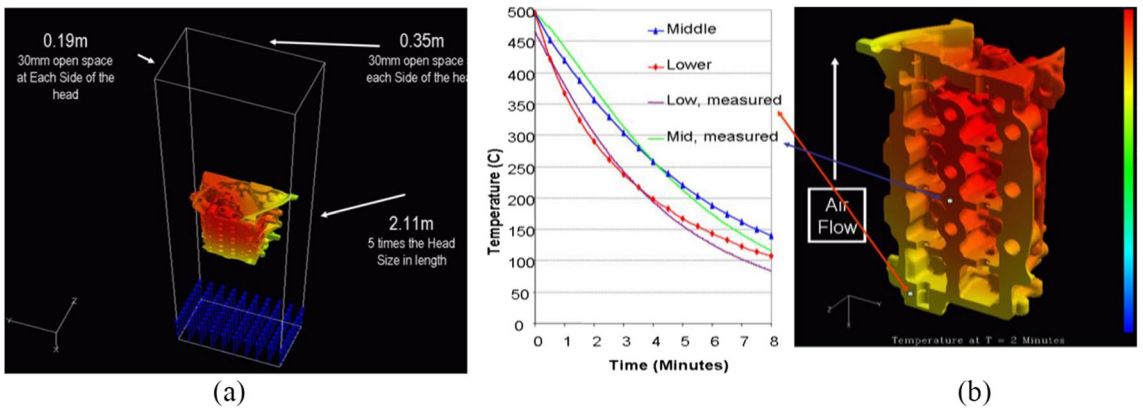

Fig. 30 **a** The cylinder head's CFD model; **b** the comparison between the predicted and measured

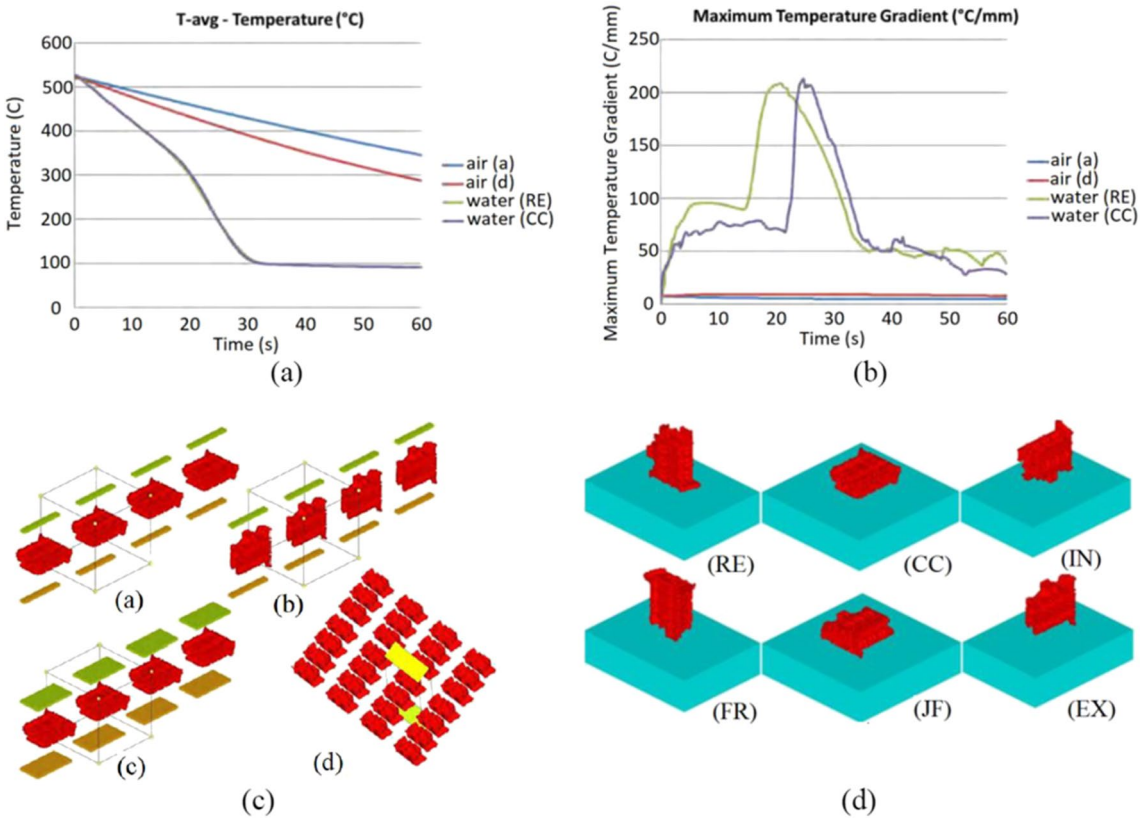

Fig. 31 The comparison between **a** the average cooling curves and **b** the maximum temperature gradient of two quenching configurations in **c** air and **d** water [21]

trial and error (the simulation results were adjusted with the experimental measurements). Temperature-dependent material thermophysical and thermomechanical properties (i.e., thermal conductivity and specific heat) were considered in the simulation and obtained from thermodynamics software (JMat Pro). The uncoupled thermo-mechanical model was

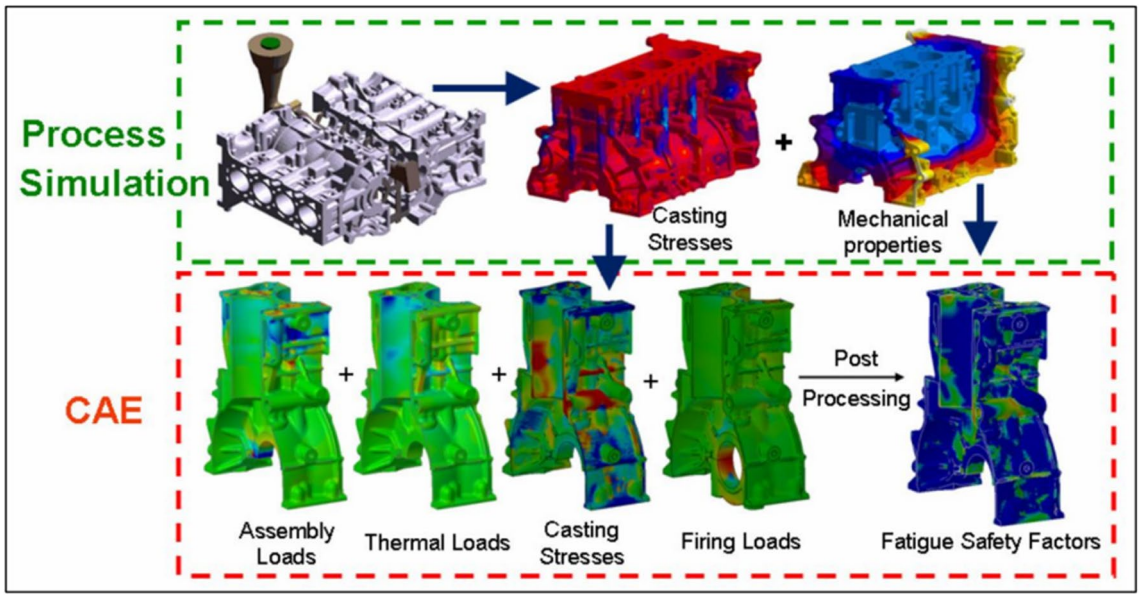

Fig. 32 The new CAE approach for engine block manufacturing developed by Ford Motor Co. [86]

Table 2 Summary of the numerical studies with the parameters and the validation methods

Specimen/Reference	Material	Casting method	Initial and boundary conditions	Validation method
Stress-lattice [78]	Al-Si alloy	HDPC	Initial die temperature: 160, 180, 200, 230, 260 °C HTC as a function of temperature	Infrared camera/measuring elongation
Stress-lattice [10]	Gray cast iron	Sand cast	Pouring temp: 1440 °C Casting initial temp (after shake out): 625 °C Sand core/sand mold: 500 ($Wm^{-2}K^{-1}$) Casting/core (HTC): 800 ($Wm^{-2}K^{-1}$)	Neutron diffraction
Stress-lattice [75]	Low-alloyed gray cast iron	Sand cast	Mold/ casting: perfect heat conduction Casing/air: 20 ($Wm^{-2}K^{-}$) Sand mold/Air (HTC): 20 ($Wm^{-2}K^{-1}$)	Strain gauge
Stress-lattice [79, 80]	Gray cast iron	Sand cast	Initial sand mold temp: 25 °C Sand mold/air: 400 ($Wm^{-2}K^{-1}$) Sand mold/casting (HTC): 400 ($Wm^{-2}K^{-1}$) Casting/air: 20 ($Wm^{-2}K^{-1}$)	Strain gauge
Engine block [82]	Al-Si alloy and gray cast iron liner	Die-cast	Heat flux between casting and air Casting initial temp: 350 °C	Coordinate measuring machine
Cylindrical Al-Si alloy casting with liner [83]	Al-Si alloy and gray cast iron liner	Similar to low-pressure die casting	Initial mold temp: 17 °C Pouring temp: 689 °C Casting/steel mold (pouring side): 2100 ($Wm^{-2}K^{-1}$) Casting/liner (HTC): 2100 ($Wm^{-2}K^{-1}$) Casting/air: 50 ($Wm^{-2}K^{-1}$) Liner/air: 42 ($Wm^{-2}K^{-1}$) Casting/steel mold (opposite pouring side): 4200 ($Wm^{-2}K^{-1}$) Steel mold/sand mold: 2100 ($Wm^{-2}K^{-1}$) Liner/steel mold: 4200 ($Wm^{-2}K^{-1}$) Casting/insulator: 4.2 ($Wm^{-2}K^{-1}$)	Thermocouple (temp. measurements) in-situ and ex-situ strain gauge measurements
I4 engine block [11]	Al-Si alloy	Sand cast	Uniform surrounding air temperature and velocity Initial temperature: 500 °C	Thermocouple/strain gauge

used in their study where the thermal and thermal-stress analyses were conducted in the CAPCAST 3.5.7 FEM software and ABAQUS commercial package, respectively. Their results revealed that the elastoplastic model overestimated the residual strain in the circumferential direction in both gray cast iron liners and Al-Si-Cu alloy casting. Furthermore, the use of the elastoplastic-creep constitutive model improved the accuracy of in-situ predictions of the circumferential strain of the liner during casting (see Figure 28) [83]. In another attempt, Motoyama et al. [84] incorporated the recovery and strain-rate dependence of the stress-strain curves into empirical elastoplastic-creep constitutive models to improve the accuracy of the thermal stress analysis of high-pressure die casting (HDPC) of the Al-Si-Cu alloy. To find the material parameters used in the constitutive equation, the authors conducted tensile tests at different temperatures, above the room temperature, to obtain stress–strain curves that most closely resemble those during or immediately after casting for the Al-Si-Cu HPDC alloy (A383.0), which exhibits natural aging. It was found that solution heat treatment with subsequent cooling to the test temperature should be applied to obtain stress–strain curves used for the thermal stress analysis of the HPDC process of the Al-Si-Cu alloy. They also conducted a comparative analysis with the aging treatment and found that the yield stresses obtained from this method were 50–64 pct. higher than the solution heat treatment which could lead to an overestimation of the predicted residual stress in die castings. Similar findings were also reported by Perzyk [85, 86] where the temperature and strain-rate history of deformation were included in constitutive models used for residual stress calculations as neglecting these effects can lead to significant errors. The Bauschinger's effect appears to be of minor importance for most of the materials and thermal loading programs (history dependant constitutive models) [85, 87]. However, the Bauschinger's effect on residual stresses of the ideal elastoplastic materials with linear hardening is significant as reported in [85, 87] (i.e., typical stress values for kinematic hardening were reduced by 30–50% in comparison with isotropic hardening).

As explained in previous sections, the cast Al-Si alloy engine blocks are required to be heat-treated before they

are put into service. The heat treatment process alters the residual stress profiles in cast components due to heating and cooling cycles in solutionizing and quenching processes. Hence, it is crucial to predict the changes in the stress patterns using FEM modelling. The following section reviews attempts made to model the heat treatment process applied to the Al-Si alloy engine block.

3.5 Finite element modelling of residual stress evolution during engine block heat treatment

Several numerical studies have been conducted to investigate the effects of heat treatment on the evolution of residual stresses in Al-Si alloy engine blocks.

Su et al. [11] developed a numerical model to predict residual stresses during quenching of a cast Al-Si alloy (A319) I4 engine block with gray cast iron liners (cast-in liners). The block was air-quenched to a lower temperature and then aged. The heat treatment procedure and the resultant cooling rate from the simulation and experimental measurement are shown in Figure 29.

Thermal analysis during the air-quench process was done using the fluent computational fluid dynamics (CFD) program. The transient temperature field was then used as thermal input to ABAQUS to calculate the resultant residual stresses. The numerical model was validated against strain gauge measurement results (Figure 29) with a good correlation with the experimental measurement data. The highest magnitude of the tensile residual stresses was found in the cylinder bridge region of the engine block [11].

Jan et al. [11, 21, 88] improved the regular heat transfer coefficient (HTC) approach for modelling the quenching process of Al-Si alloy cylinder heads. Since the HTC is dependent on geometry, temperature, time, and flow in typical convective heat transfer conditions, the HTC values will change by changing any of these parameters. Therefore, the conventional HTC calculation methods need to be repeated when any of these parameters are changed, resulting in lengthy and costly experiments. In the new approach, the CFD technique was employed to solve heating equations in the solid and liquid in conjunction with the flow equation at the same time to calculate the HTC at the casting-quenchant interface. Then, they verified the model by applying it to the air-quenching process of an Al-Si alloy cylinder head and comparing the calculated results with the experiment, as shown in Figure 30.

They also studied the effects of quenching orientation and media, i.e., water and air, on the Al-Si alloy cylinder head cooling process. Based on their study, quenching orientation has a negligible effect on the component's temperature gradient and total cooling rate, as can be seen in Figure 31. Nevertheless, though the effect of quenching configuration and orientation on the HTC was explored, the residual stresses were not predicted. They also found that the HTC remains almost constant during the air-quench process for all quench configurations. From their results, it can be concluded that this novel approach is an effective and accurate way to determine the casting-quenchant interface's HTC during the quenching process without the need to conduct typical HTC evaluation/calibration experiments. However, this method can only be employed to model pure convection heat transfer problems and it is not applicable to solidification modelling, where a combination of all three heat transfer mechanisms is active. Furthermore, since the model solves many boundary condition equations simultaneously, it requires high computational resources to simulate the quenching process of large complex components like engine blocks.

In the previous numerical studies, the casting/solidification stage and the heat treatment stage of the engine blocks were separately modelled to predict residual stresses. However, some studies developed numerical models to predict the evolution of the residual stress in Al-Si alloy engine blocks due to both solidification and the subsequent heat treatment processes. In Menne et al. [89], some engine projects from Ford showed the importance finite element modelling of casting and heat treatment processes to predict the final mechanical properties, residual stress distribution, and potential defects. A combination of the predicted residual stress profiles, operating loads, and assembly was used in fatigue analysis to examine the engine's durability during service, as shown in Figure 32. They concluded that FEM modelling of the casting process as a part of the CAE before engine block manufacturing can significantly cut the technology development phase's time and cost (by up to 50%) and improve the products' quality and durability. The MAGMA commercial package was used for the analysis; however, the modelling parameters such as boundary conditions or material properties were not discussed in the report.

Table 2 summarizes the conducted numerical studies with the simulation parameters and their experimental validation methods.

Finite element modelling of residual stresses requires accurate temperature-dependent material properties, an accurate thermal history, and some method of benchmarking the analysis technique; typically using a simpler sample such as the stress lattice. There are considerable savings in cost and time when this is performed as part of the design process, as problem areas can be identified before prototyping.

4 Conclusions

This paper presents a review of numerical and experimental measurement techniques to evaluate residual stresses in engine blocks. Several key examples of both numerical simulations and experimental measurement techniques of residual

stresses were reviewed in different manufacturing stages of the manufacturing process of Al-Si alloy engine blocks.

Among many possible measurement techniques, sectioning and neutron diffraction are widely used to characterize bulk residual stresses in the engine block. In this paper, the principle and critical issues in both sectioning and neutron diffraction methods were summarized, along with several case studies to determine the residual stresses in the engine blocks. Despite the fact that the sectioning method is an accurate and economical technique to evaluate residual stresses within thin plates, this method provides only limited information on the nature of the stresses within a component and could be utilized for surface measurements and qualitative analyses only. On the other hand, neutron diffraction is a high precision non-destructive technique, with $\pm 50 \times 10^{-6}$ accuracy in strain with > 0.1 mm spatial resolution, capable of characterizing bulk residual stresses in all three principal direction at many locations within the block at different stages of the manufacturing process as well as the relaxation of residual stresses during heat treatment of the engine block.

The case studies of in situ neutron diffraction measurements were described, and the results were discussed in this paper. The residual stress variations were also discussed in conjunction with microstructural and mechanical properties of the engine block.

The numerical case studies included benchmark studies and residual stress evolution during engine block solidification as well as heat treatment. Different approaches were used for the developed numerical models (i.e., plasticity or thermo-physical models) which require proper validating through experimental measurements for each investigation.

Acknowledgements The authors would like to sincerely appreciate the support provided by Dr. Dimitry Sediako for reviewing and providing feedback on the paper.

Declarations

Ethics approval Not applicable

Consent to participate All authors give consent to participate in the study and its subsequent publication.

Consent for publication All authors consent to publication.

Conflict of interest The authors declare no competing interests.

References

1. Hauk V (1997) Structural and residual stress analysis by nondestructive methods. Elsevier, Oxford
2. Barsoum Z, Barsoum I (2009) Residual stress effects on fatigue life of welded structures using LEFM. Eng Fail Anal 16:449–467
3. Sim W-M (2010) Challenges of residual stress and part distortion in the civil airframe industry. Int J Microstruct Mater Prop 5:446–455
4. Withers PJ, Bhadeshia H (2001) Residual stress. Part 1–measurement techniques. Mater Sci Technol 17:355–365
5. Farhangi H, Norouzi S, Nili-Ahmadabadi M (2004) Effects of casting process variables on the residual stress in Ni-base superalloys. J Mater Process Technol 153:209–212
6. Withers PJ (2007) Residual stress and its role in failure. Reports Prog Phys 70:2211
7. Smith M, Levesque J-B, Bichler L, Sediako D, Gholipour J, Wanjara P (2017) Residual stress analysis in linear friction welded in-service Inconel 718 superalloy via neutron diffraction and contour method approaches. Mater Sci Eng A 691:168–179
8. Mohamed SS, Samuel AM, Doty HW, Valtierra S, Samuel FH (2019) Relation between residual stresses and microstructure evolution in Al–Si alloys based on different casting parameters. Philos Mag 99:284–305
9. Dini H, Andersson NE, Jarfors AE (2020) Effect of process parameters on distortion and residual stress in high-pressure die cast AZ91D components after clean blasting and painting. Int J Metalcast 15:241–258
10. Johnson EM, Watkins TR, Schmidlin JE, Dutler SA (2012) A benchmark study on casting residual stress. Metall Mater Trans A 43:1487–1496
11. Su X, Jan J, Lasecki J, Allison J (2003) Thermal and residual stress analysis of an engine block with cast-in liners. Mater Solut Confer 2003:63–68
12. Carrera E, Rodriguez A, Talamantes J, Valtierra S, Colas R (2007) Measurement of residual stresses in cast aluminium engine blocks. J Mater Process Technol 189:206–210
13. Stroh J, Piche A, Sediako D, Lombardi A, Byczynski G (2019) The effects of solidification cooling rates on the mechanical properties of an aluminum inline-6 engine block. In: Light Metals. Springer International Publishing, Cham, pp 505–512
14. Mehr FF, Cockcroft S, Reilly C, Maijer D (2020) Investigation of the efficacy of a water-cooled chill on enhancing heat transfer at the casting-chill interface in a sand-cast A319 engine block. J Mater Processing Technol 286:116789
15. Schajer GS (2013) Practical residual stress measurement methods. John Wiley & Sons, Chichester, United Kingdom
16. Rossini NS, Dassisti M, Benyounis KY, Olabi A-G (2012) Methods of measuring residual stresses in components. Mater Des 35:572–588
17. Fitzpatrick ME, Lodini A (2003) Analysis of residual stress by diffraction using neutron and synchrotron radiation, CRC Press.
18. Hutchings MT (2005) Introduction to the characterization of residual stress by neutron diffraction, CRC press.
19. Allen AJ, Hutchings MT, Windsor CG, Andreani C (1985) Neutron diffraction methods for the study of residual stress fields. Adv Phys 34:445–473

20. Withers PJ, Turski M, Edwards L, Bouchard PJ, Buttle DJ (2008) Recent advances in residual stress measurement. Int J Press Vessel Pip 85:118–127
21. Jan J, Nannapuraju M (2017) CFD investigation of quench media and orientation effects on structural stress induced in the intense quenching processes for aluminum cylinder heads. In: ASM 29th Heat Treat Soc Conf. Expo. 24–26. ASM International, Columbus, OH, pp 411–421
22. Aguilar-Navarro JA, González-López JR, Hernández-Sandoval J, Berber-Solano TP, Castillo-Morales M, González-Villareal JA, Salas-Zamarripa A, Castillo-Elizondo JA (2020) Innovative methodology for measuring residual stress in engine blocks. Int J Adv Manuf Technol 106:3649–3658
23. Lombardi A, Sediako D, Machin A, Ravindran C, MacKay R (2015) Transient analysis of residual strain during heat treatment of multi-material engine blocks using in-situ neutron diffraction. Mater Lett 157:50–52
24. Huang X, Liu Z, Xie H (2013) Recent progress in residual stress measurement techniques. Acta Mech Solida Sin 26:570–583
25. Hosseinzadeh F, Kowal J, Bouchard PJ (2014) Towards good practice guidelines for the contour method of residual stress measurement. J Eng 2014:453–468
26. Dean J, Gu T, Clyne TW (2015) Evaluation of residual stress levels in plasma electrolytic oxidation coatings using a curvature method. Surf Coatings Technol 269:47–53
27. Schajer GS (2010) Advances in hole-drilling residual stress measurements. Exp Mech 50:159–168
28. Zhao L, Macías JGS, Dolimont A, Simar A, Rivière-Lorphèvre E (2020) Comparison of residual stresses obtained by the crack compliance method for parts produced by different metal additive manufacturing techniques and after friction stir processing. Addit Manuf 36:101499
29. Korsunsky AM, Sebastiani M, Bemporad E (2009) Focused ion beam ring drilling for residual stress evaluation. Mater Lett 63:1961–1963
30. Jandera M, Machacek J (2010) Residual stress pattern of stainless steel SHS. In: Tubul. Struct. XIII-Proc. 13th Int. Symp. Tubul. Struct, pp 265–272
31. Young B, Lui W-M (2005) Behavior of cold-formed high strength stainless steel sections. J Struct Eng 131:1738–1745
32. Kianfar S, Aghaie E, Stroh J, Sediako D, Tjong J (2020) Residual stress, microstructure, and mechanical properties analysis of HPDC aluminum engine block with cast-in iron liners. Mater Today Commun 26:101814
33. Salem Mohamed S (2018) Effects of metallurgical parameters on the development of residual stresses in Al-Si alloys used in engine block manufacturing. Université du Québec à Chicoutimi
34. Mohamed SS, Samuel AM, Doty HW, Valtierra S, Samuel FH (2020) Development of residual stresses in Al–Si engine blocks subjected to different metallurgical parameters. Int J Met 14:25–36
35. Dieter GE (1986) Mechanical Metallurgy, 3rd edn. McGraw-Hill, Boston, MA
36. Lombardi A, Sediako D, Machin A, Ravindran C, MacKay R (2017) Effect of solution heat treatment on residual stress in Al alloy engine blocks using neutron diffraction. Mater Sci Eng A 697:238–247
37. Rincon E, Lopez HF, Cisneros MM, Mancha H (2009) Temperature effects on the tensile properties of cast and heat treated aluminum alloy A319. Mater Sci Eng A 519:128–140
38. Rajaram G, Kumaran S, Rao TS (2011) Effect of graphite and transition elements (Cu, Ni) on high temperature tensile behaviour of Al–Si Alloys. Mater Chem Phys 128:62–69
39. Zheng B, Shu G, Jiang Q (2019) Experimental study on residual stresses in cold rolled austenitic stainless steel hollow sections. J Constr Steel Res 152:94–104
40. Ravi B (1999) Computer-aided casting design–past, present and future. Korea 1:777
41. Alipooramirabad H, Paradowska A, Lavigne O, Ghomashchi R, Reid M (2017) In situ neutron diffraction measurement of strain relaxation in welds during heat treatment. Sci Technol Weld Join 22:484–495
42. Pratt P, Felicelli SD, Wang L, Hubbard CR (2008) Residual stress measurement of laser-engineered net shaping AISI 410 thin plates using neutron diffraction. Metall Mater Trans A 39:3155–3163
43. Sediako D, D'Elia F, Lombardi A, Machin A, Ravindran C, Hubbard C, Mackay R (2011) Analysis of residual stress profiles in the cylinder web region of an As-Cast V6 Al engine block with cast-in Fe liners using neutron diffraction. SAE Int J Mater Manuf 4:138–151
44. Alipooramirabad H, Paradowska A, Reid M, Ghomashchi R (2022) Effect of holding time on strain relaxation in high-strength low-alloy steel welds: an in-situ neutron diffraction approach. J Manuf Process 73:326–339. https://doi.org/10.1016/j.jmapro.2021.11.005
45. Woo W, Feng Z, Wang X, David SA (2011) Neutron diffraction measurements of residual stresses in friction stir welding: a review. Sci Technol Weld Join 16:23–32
46. Webster GA, Wimpory RW (2001) Polycrystalline materials—determinations of residual stresses by neutron diffraction. ISO/TTA3 Technology Trends Assessment, Geneva, p 20
47. Noyan IC, Cohen JB (2013) Residual stress: measurement by diffraction and interpretation. Springer, New York, NY
48. Vogel SC, Priesmeyer H-G (2006) Neutron production, neutron facilities and neutron instrumentation. Rev Mineral Geochemistry 63:27–57
49. Hurd AJ, Schaefer DW (2006) Introduction to materials and bioscience neutron-scattering research. Los Alamos Sci 30:146
50. Alipooramirabad H, Paradowska A, Reid M, Ghomashchi R (2022) Effects of PWHT on the residual stress and microstructure of bisalloy 80 steel welds. Metals (Basel) 12(10):1569
51. Lombardi A, Vandersluis E, Sediako D, Ravindran C (2017) Neutron diffraction analysis of light alloys: a review. In: Materials Science Forum, vol 879. Trans Tech Publications Ltd., Switzerland, pp 1558–1563
52. Pynn R (2009) Neutron scattering—a non-destructive microscope for seeing inside matter. In: Neutron applications in earth, energy and environmental sciences. Springer, pp 15–36. https://doi.org/10.1007/978-0-387-09416-82
53. Withers PJ (2007) Mapping residual and internal stress in materials by neutron diffraction. Comptes Rendus Phys 8:806–820
54. Lombardi A (2011) A study of cylinder bore distortion in V6 aluminum alloy engine blocks. Master Applied Science Thesis, Ryerson University, Toronto, ON
55. Sediako D, D'Elia F, Lombardi A, Machin A, Ravindran C, Hubbard C, Mackay R (2011) Application of neutron diffraction in analysis of residual stress profiles in the cylinder web region of an as-cast V6 Al engine block with cast-in Fe liners. Suppl Proc Mater Fabr Prop Charact Model 2:299–308
56. Lombardi A, Ravindran C, Sediako D, MacKay R (2014) Determining the mechanism of in-service cylinder distortion in aluminum engine blocks with cast-in gray iron liners. Metall Mater Trans A 45:6291–6303
57. Lados DA, Apelian D, Wang L (2010) Minimization of residual stress in heat-treated Al–Si–Mg cast alloys using uphill quenching: mechanisms and effects on static and dynamic properties. Mater Sci Eng A 527:3159–3165
58. Rolph J, Evans A, Paradowska A, Hofmann M, Hardy M, Preuss M (2012) Stress relaxation through ageing heat treatment–a comparison between in situ and ex situ neutron diffraction techniques. Comptes Rendus Phys. 13:307–315
59. Lombardi A, D'Elia F, Ravindran C, Sediako D, Murty BS, MacKay R (2012) Interplay between residual stresses, microstructure,

process variables and engine block casting integrity. Metall Mater Trans A 43:5258–5270
60. Lombardi A, Ravindran C, MacKay R (2014) Improvements in mechanical properties of 319 Al alloy engine blocks through cost-effective solution heat treatment. J Mater Eng Perform 23:2766–2771
61. Lombardi A, Ravindran C, MacKay R (2015) Optimization of the solution heat treatment process to improve mechanical properties of 319 Al alloy engine blocks using the billet casting method. Mater Sci Eng A 633:125–135
62. Ahmad S, Sediako D, Lombardi A, Ravindran CR, Mackay R, Nabawy A (2016) Assessment of residual stress in T5 treated 319 aluminum alloy engine blocks using neutron diffraction (No. 2016-01-0353). SAE Technical Paper
63. Godlewski LA, Su X, Pollock TM, Allison JE (2013) The effect of aging on the relaxation of residual stress in cast aluminum. Metall Mater Trans A 44:4809–4818
64. Liu T, Brewer LN, Bunn JR, Fancher CM, Nastac L, Arvikar V, Levin I (2019) Measurement of residual strain in the cylinder bridge of high-pressure die cast A383 engine blocks using neutron diffraction. In: Shape Casting: 7th International Symposium Celebrating Prof. John Campbell's 80th Birthday. Springer International Publishing, pp 303–310. https://doi.org/10.1007/978-3-030-06034-3_29
65. Liu T, Bunn JR, Fancher CM, Nastac L, Arvikar V, Levin I, Brewer LN (2020) Neutron diffraction analysis of residual strain in high-pressure die cast A383 engine blocks. J Mater Eng Perform 29:5428–5434
66. Stroh J, Sediako D, Byczynski G, Lombardi A (2020) Paradowska, Stress characterization of bore-chilled sand cast aluminum engine blocks in As-cast and T7 condition with application of neutron diffraction. In: Light Metals 2020. Springer International Publishing, pp 153–157
67. Stroh J, Sediako D, Lombardi A, Byczynski G, Reid M, Paradowska A (2022) Evolution of residual stress through the processing stages in manufacturing of bore-chilled sand-cast aluminum engine blocks with pressed-in iron liners. Int J Adv Manuf Technol 120:4693–4705
68. Lewis RW, Ravindran K (2000) Finite element simulation of metal casting. Int J Numer Methods Eng 47:29–59
69. Choudhari CM, Padalkar KJ, Dhumal KK, Narkhede BE, Mahajan SK (2013) Defect free casting by using simulation software. Appl Mech Mater 313:1130–1134.C
70. Shepel SV, Paolucci S (2002) Numerical simulation of filling and solidification of permanent mold castings. Appl Therm Eng 22:229–248
71. McClory B, Nguyen W, Heisser C (2010) Effect of simulated material properties and residual stresses on high cycle fatigue prediction in a compacted graphite iron engine block (No. 2010-01-0016). SAE Technical Paper
72. Acharya SG, Vadher JA, Sheladiya MV, Madhnani M (2016) Quality casting of motor body using design of experiment and casting simulation. Int J Manuf Res 11:111–125
73. Rappaz M (1989) Modelling of microstructure formation in solidification processes. Int Mater Rev 34:93–124
74. Prakash SA, Hariharan C, Arivazhagan R, Sheeja R, Raj VAA, Velraj R (2021) Review on numerical algorithms for melting and solidification studies and their implementation in general purpose computational fluid dynamic software. J Energy Storage 36:102341
75. Gustafsson E, Hofwing M, Strömberg N (2009) Residual stresses in a stress lattice—Experiments and finite element simulations. J Mater Process Technol 209:4320–4328
76. Inoue Y, Motoyama Y, Takahashi H, Shinji K, Yoshida M (2013) Effect of sand mold models on the simulated mold restraint force and the contraction of the casting during cooling in green sand molds. J Mater Process Technol 213:1157–1165
77. Metzger D, New KJ, Dantzig J (2001) A sand surface element for efficient modeling of residual stress in castings. Appl Math Model 25:825–842
78. Hofer P, Kaschnitz E, Schumacher P (2014) Distortion and residual stress in high-pressure die castings: simulation and measurements. Jom 66:1638–1646
79. Motoyama Y, Inukai D, Okane T, Yoshida M (2014) Verification of the simulated residual stress in the cross section of gray cast iron stress lattice shape casting via thermal stress analysis. Metall Mater Trans A 45:2315–2325
80. Motoyama Y, Takahashi H, Okane T, Fukuda Y, Yoshida M (2013) Numerical and experimental study on residual stress in gray cast iron stress lattice shape casting. Metall Mater Trans A 44:3261–3270
81. Sediako D, Sediako O, Lin KJ (1999) Some aspects of thermal analysis and technology upgrading in steel continuous casting. Can Metall Q 38:377–385
82. Ahlström J, Larsson R (2012) Modeling of distortion during casting and machining of aluminum engine blocks with cast-in gray iron liners. Mater Perform Charact 1:1–19
83. Motoyama Y, Ebihara N, Shiga H, Sato T, Kambe H, Yoshida M (2018) Thermal stress analysis of residual stress in a cylindrical aluminum casting with cast-in GCI liner, taking recovery behavior effect into account. Metall Mater Trans A 49:5619–5635
84. Motoyama Y, Shiga H, Sato T, Kambe H, Yoshida M (2016) Elasto-plastic-creep constitutive equation of An Al-Si-Cu high-pressure die casting alloy for thermal stress analysis. Metall Mater Trans A 47:5598–5608
85. Perzyk MA (1989) The role of deformation history effects in generation of residual thermal stresses. In: International Conference on Residual Stresses: ICRS2. Springer, Netherlands, pp 454-459
86. Perzyk MA (1985) Validity of constitutive equations used for calculation of stresses in cooling castings. Mater Sci Technol 1:84–92
87. Perzyk M (1987) A constitutive model for deformation of metals over wide temperature ranges. Comput Plast Model Softw Appl Part I:563–576
88. Su X, Lasecki J, Jan J, Engler-Pinto C Jr, Allison J (2009) Residual stress analysis of air–quenched engine aluminum cylinder heads. SAE Int J Engines 1:1015–1019
89. Menne RJ, Weiss U, Brohmer A, Egner-Walter A, Weber M, Oelling P (2007) Implementation of casting process simulation for increased engine performance and reduced development time and costs-selected examples from FORD R and D engine projects. In: Proceedings of the 28th International Vienna Motor Symposium. IVMS, Vienna, Austria